2006

Petrological and geochemical investigations of deep sea turbidite sands in the Pandora and Moresby Troughs: Source to Sink Papua New Guinea Focus Area

Luke Jeremiah Patterson
Louisiana State University and Agricultural and Mechanical College

PETROLOGICAL AND GEOCHEMICAL INVESTIGATIONS OF DEEP SEA TURBIDITE SANDS IN THE PANDORA AND MORESBY TROUGHS: SOURCE TO SINK PAPUA NEW GUINEA FOCUS AREA

A Thesis
Submitted to the Graduate Faculty of the
Louisiana State University and
Agricultural and Mechanical College
in partial fulfillment of the
requirements for the degree of
Master of Science

in

The Department of Oceanography and Coastal Sciences

by
Luke Patterson
B.S., Louisiana State University, 2003
May 2006

ACKNOWLEDGMENTS

I would like to thank Dr. Sam Bentley for endless amounts of support, patience, and guidance through a challenging yet fulfilling research endeavor. Dr. Bentley has gone above and beyond his duty as an advisor and he quickly became a mentor as well as a lifetime friend. Thesis committee member Dr. Darrell Henry whom unknowingly precipitated at least in part a petrological and geochemical based project after my exit from his Igneous and Metamorphic course, and who aided considerably in the written work. Thesis committee member Dr. Bob Carney who contributed through many insightful conversations. All of the 2004 Panash PI's and cruise members who aided in the acquisition of samples, and for great companionship while aboard the RV-Melville. Special thanks to fellow cruise members and companions here at LSU, Lawrence Febo, Zahid Muhammad, and Floyd Demers for assistance before, during, and post cruise. Many thanks go to Rick Young and Dr. Xiaogang Xie for assistance with sample preparation and microanalysis. Thanks to the Louisiana State University Department of Oceanography and Coastal Sciences as a whole for support and contributions of the faculty and staff, especially Gaynell Gibbs for administrative assistance. Thanks to Erica Picou for the contributions to the industry recruitment program. Thanks to my wife Harmony for her unparalleled support and wonderful ability in raising our children and providing a stable home environment in which all else is able to fall into place. Much thanks to fellow lab mates; Kristi Rotondo, Brian Velardo, Triniti Dufrene, and Skylar Neylon whom helped pave the way and created a lively office environment. Support for this research was provided by The National Science Foundation (Award No. 0305373) as part of NSF-MARGINS Source-to-Sink Initiative in the Papua New Guinea region.

TABLE OF CONTENTS

LIST OF FIGURES

ABSTRACT

The Moresby and Pandora Troughs of the northern Coral Sea are components of the deep-sea depositional system that is the ultimate sink for the Source to Sink Papua New Guinea (PNG) Focus Area. Cores collected from the R/V Melville during March-April 2004 reveal marine volcaniclastic and terrigenous turbidites deposited in these troughs during the Quaternary. Constraining the spatial, temporal, and provenance characteristics for these terrigenous sands through mineralogical, chemical, and textural analysis is the primary focus of this study.

All cores contain thinly-bedded sandy turbidite packages interlayered with hemipelagic marls and typical centimeter-to-meter-thick turbidite sequences. The Moresby Trough core JPC22 appears to be generally finer-grained then the Pandora trough core JPC 66. Typical QFL percentages from JPC22 are 13:65:23, respectively, and plagioclase/ total feldspar ratios are near 0.90. These basal turbidite sands contain well-preserved rhyolitic pumice fragments and glass shards, with phenocrysts of amphibole, plagioclase, biotite, pyroxene and oxides. Typical QFL percentages from Pandora Trough core JPC66 are 69:14:17, and plagioclase / total feldspar ratios are near 0.47. These basal turbidite sands are predominantly quartzofeldspathic with a significant amount of heavy minerals (zircon, amphibole and oxides). The contrast in submarine sand mineralogy and mineral chemistry between 66JPC and 22JPC reflects distinct sedimentary sources composed of both fluvial and volcaniclastic material. The Moresby Trough has received secondary monomagmatic volcaniclastic turbidite sands derived mostly from volcanic/collision margin highlands of SE PNG, and the Pandora Trough has received quartzo-feldspathic sands from the Fly/Strickland system, more akin to a trailing-edge margin. Mineral textures and chemistry suggests minimal associations between sand bodies, and may represent isolated basins controlled by complex sea-floor bathymetry and episodic turbidity flows from diverse sources.

The signature of the adjacent submarine fan deposits may aid the interpretation of continental margin growth as a function of sediment flux, sediment source, and dispersal pathways. These deposits may also give insight into the evolution of volcanic island arcs on longer time scales. This investigation concludes that the Pandora and Moresby trough turbidite sand bodies record varying sediment sources and somewhat isolated volcanic events contributing to the evolution of the southern PNG continental margin.

INTRODUCTION

Deep-sea turbidite deposits can provide evidence of the nature of the pre-eroded parent rock and the tectonic history of the adjacent orogenic belt. Sediment compositions are influenced by the character of the sedimentary provenance, the nature of the sedimentary processes within the depositional basin, and the kind of dispersal paths that link source to basin (Dickenson and Suczek, 1979). Weltje and Von Eynatten (2004) presented a holistic review of quantitative provenance analysis of sediments, in which they state: "successful provenance analysis requires that the nature and extent of compositional and textural modifications to the detrital spectrum be recognized, if not quantified". New developments in technology have allowed geochemists to analyze individual minerals or rock fragments such as those seen in fine-grained sandy turbidites in hopes of chemically fingerprinting the source of the original rock (Weltje and Von Eynatten, 2004; Whitmore et al, 2004 etc). The multi-disciplinary approach undertaken in this study of the turbidites of the Gulf of Papua (GOP) has been guided by both traditional and contemporary approaches and techniques.

The investigation of the GOP turbidites builds on comparable quantitative investigations of provenance sources of turbidites, ranging from unconsolidated modern river samples to outcrops of ancient turbidites. For example, Schneider et al. (2001) worked on sedimented foreland basin rocks on the Mahia peninsula (North Island, New Zealand). Using geochemical analyses of glass shards from volcaniclastic sands they defined three distinct types of turbidite deposits associated with pyroclastic flows that enter the ocean: 1) primary monomagmatic turbidites, 2) secondary monomagmatic turbidites, and 3) secondary multimagmatic turbidites. Each of these types displays variation within the volcanic glass representative of storage on the shelf versus immediate deposition in the deep sea and also single versus multiple magmatic events within the same region. Conceptually the New Zealand turbidite sediments (Schneider et

al. 2001) and their storage on the shelf and transfer into the deep sea may be analogous to the modern turbiditic sequences seen in the GOP.

In an earlier study of 27 gravel, sand and mud samples from the same locality in Northern Papua New Guinea the mineralogical and geochemical variation as a function of grain size was examined by Whitmore et al. (2004). They concluded that detailed petrographic analysis of grain types, as opposed to recalculated modal or geochemical data, is required to elucidate both upper and lower plate provenances, and discriminate between ancient and contemporary arc provenances. Due to the fine-grained nature of the turbidites in the GOP, analysis was limited only to the very fine sand fraction (63-125 μm). The restricted grain size in the GOP is important because it limits the grain size factors associated with modal analyses (Potter, 1978).

The primary focus of this study is on the basal turbidite sands from selected sites on the continental slope and rise of the Gulf of Papua and on the geochemistry of characteristic and diagnostic minerals found in these sands. Detrital quartz, feldspar, amphibole, biotite and volcanic glass are common constituents that are deposited as detrital grains in clastic sediments. The general identification, textures and modal analysis of clastic constituents can provide insights into the provenance of the clastic sediments. However, quantitative chemical analysis of these grains can more accurately define provenance. The objectives of this investigation are to: 1) characterize and interpret the compositional variability of the modern turbidite sand bodies within the Pandora and Moresby troughs, Gulf of Papua; 2) reconstruct and interpret the history of sediments from the initial erosion of parent rocks to the final burial of their detritus; and 3) deduce the characteristics of source areas from measurements of compositional, geochemical, and textural properties of sediments, supplemented by information from other lines of evidence (e.g. regional geology, drainage patterns, oceanographic processes, and stratigraphic framework).

GEOLOGIC SETTING

Evolution of the Island Arc

Papua New Guinea (PNG) is part of a complex convergent plate boundary between the Indo-Australian Plate, the Pacific plate, and several other smaller plates including the Philippine Sea and Caroline Plates (Fig. 1). "Tectonic uplift" along the collision margin has produced significant relief (> 4 km) in PNG; this relief, coupled with high precipitation in this tropical region (2-10 m/yr), produces runoff that carries abundant sediment downstream (NSF MARGINS S2S, 2004). This tectonic setting has created an active volcanic island arc, composed of diverse rock types, many of which contribute sediments to the back-arc basin setting. More than 300 x 10^6 metric tons of sediment arrives annually at the mouth of the rivers entering the GOP, including the Fly, Kikori, and Purari, which are the largest sources (Milliman, 1995). This suspended sediment discharge is greater then that of the Mississippi river (230 x 10^6 metric tons), which ranks among the worlds top ten. However, fluvial discharges of water and sediment are poorly constrained, especially in the area of the high mountains of eastern PNG, a region with large areas of drainage but small drainage basins. An additional delivery mechanism in this region could be related to slope failure, especially during periods of torrential precipitation. Landsliding is increasingly appreciated as a major control on landscape development in mountainous terrains (Hovius, 2000).

Resulting Topography and Bathymetry

The geomorphology of the southern New Guinea continental shelf varies dramatically, from the west where much of the sediment is presumably trapped as a prograding clinoform on a broad shelf, to the east where the shelf narrows (< 10 km) allowing fluvial sediment to escape directly to the adjacent deep sea (Milliman, 1995).

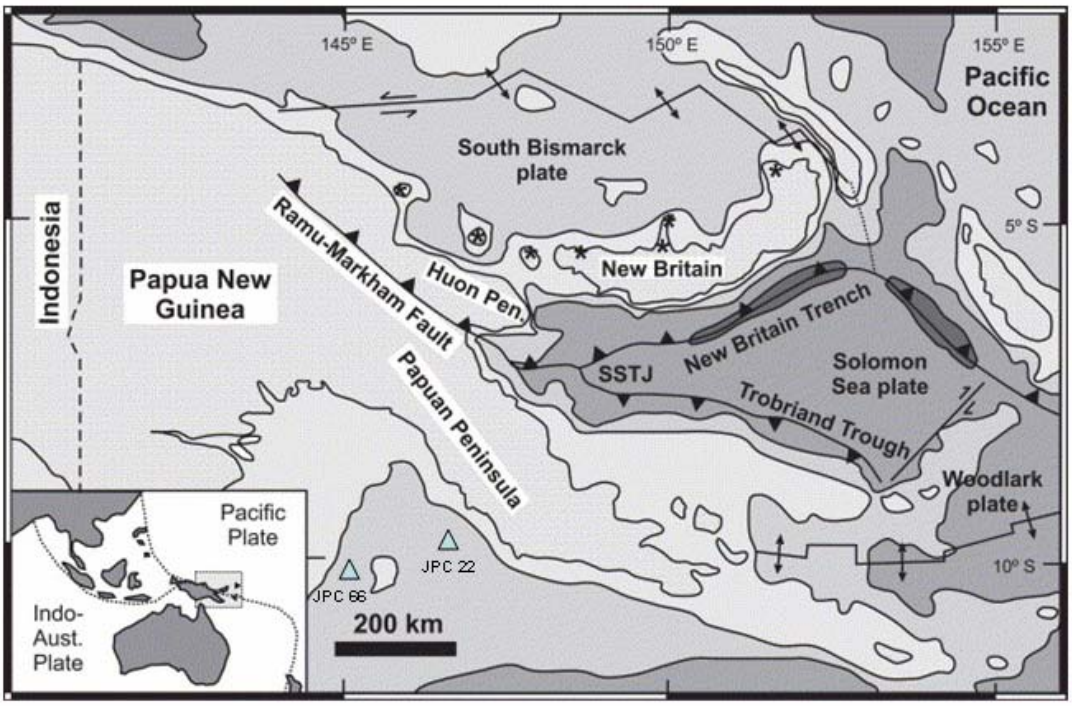

Figure 1. Regional tectonic setting of the PNG study area. Arc-continent collision between the underthrust Indo-Australian plate and overriding South Bismarck plate is taking place to the west of the Solomon Sea triple junction (SSTJ). To the east, the Solomon Sea plate is being subducted northwards rapidly along the New Britain trench and more slowly southwards along the Trobriand trough. Stars mark active volcanoes, triangles mark the direction of underthrusting along the New Guinea collision, and bathymetric contours indicate 1, 3 and 7 km (Whitmore et al, 2004). Upward triangles with sample numbers mark approximate core locations. Note that the core locations for this study are in a relatively quiet tectonic setting, despite being adjacent to a collisional margin.

The regional hinterland geology is not well described, and only a crude geologic map can provide the outcrop lithologies for correlating sediments to their detrital parents (Steinshouer et al. 1999) (Figure 2). There is strong evidence for Pleistocene volcanism in the Fly-Highlands province of western PNG, where the rocks are interpreted as uncontaminated, mantle-derived magmas. This volcanism is presumably associated with the Pliocene crustal uplift that caused the development of the highlands following a mid-Tertiary continent/island-arc collision. In this region a wide range of Pleistocene volcanic rocks has been identified, ranging from alkali to tholeiitic basalt, basanite, trachybasalt and andesite (Hamilton et al. 1983).

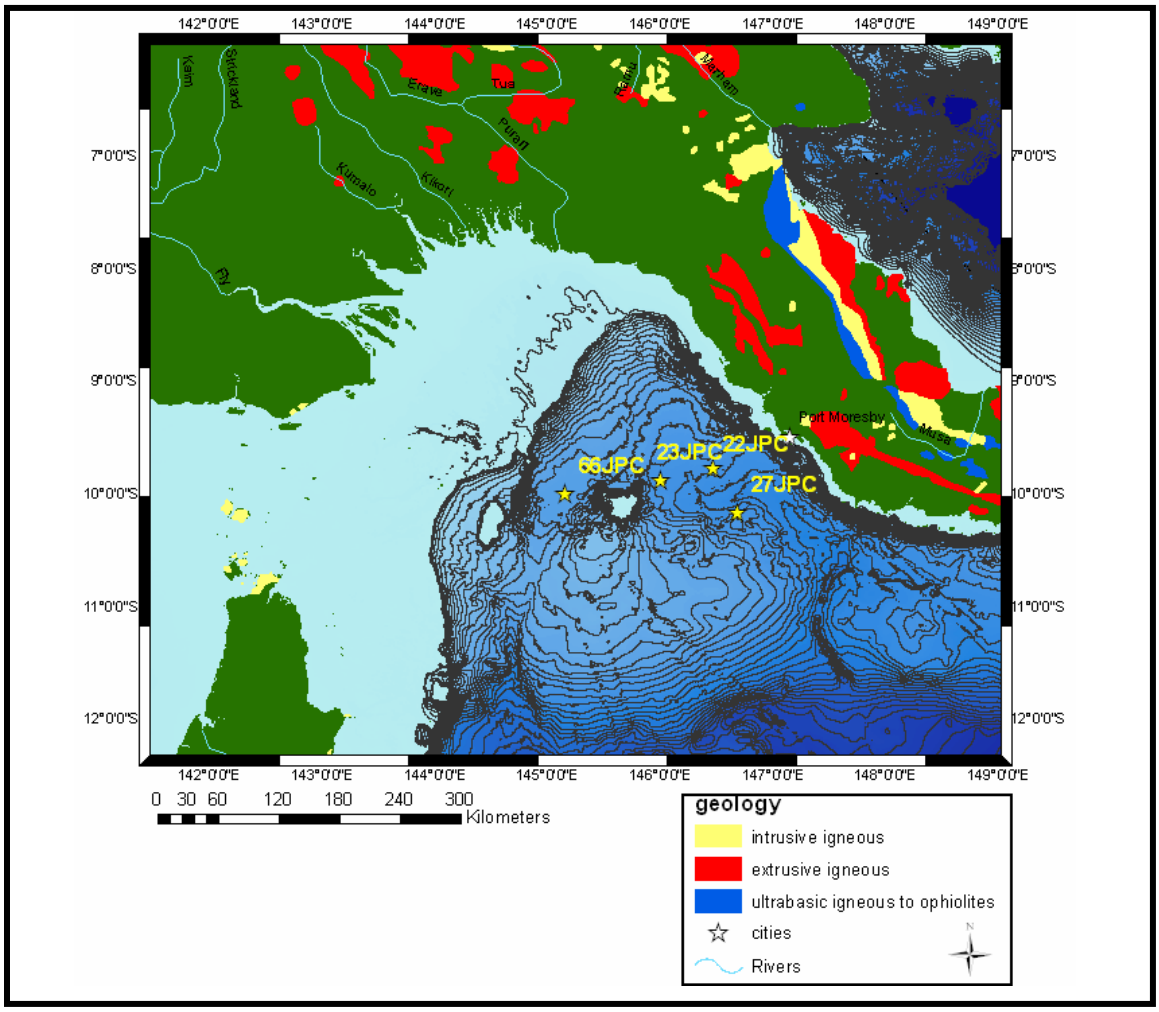

Figure 2. Generalized lithologies of PNG hinterlands: red = volcanics, yellow = intrusive, blue = ultramafic; green colored areas represent varying aged sedimentary covers (Steinshouer et al. 1999). Colored multibeam lines were acquired aboard cruise and represent basin bathymetry in the GOP.

General Morphology of the Pandora and Moresby Troughs

The Pandora Trough lies between the eastern slope of the Ashmore-Boot-Portlock Reef complex, the broad south-central PNG shelf margin, and the western slope of the Eastern Plateau. This trough is open to the northeast where the Moresby Canyon connects the Pandora trough to the western Coral Sea abyssal plain and to the south where most of the sediment escapes (Fig. 3).

The Moresby trough is morphologically more poorly-defined, representing a large portion of the deep Gulf of Papua, and is the primary conduit for sediment dispersal into the

deeper basins of the Coral Sea. This portion of the basin lies between the eastern slope of the Eastern Plateau and the narrow southeastern PNG shelf margin (Fig. 3).

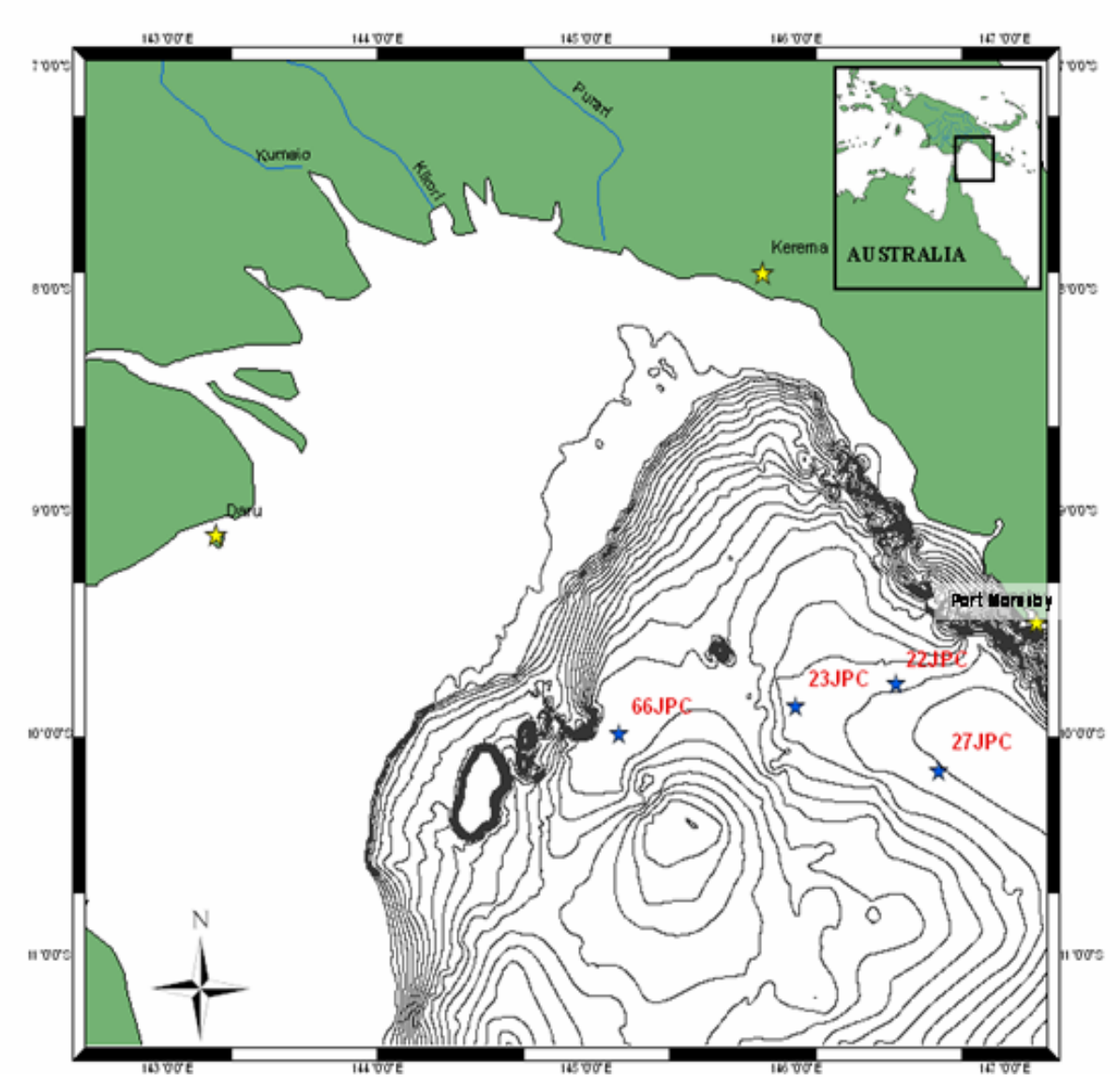

Figure 3. Study area with representative core locations represented as blue stars. Town locations represented as yellow stars. Bathymetric contours are 100m resolution. Dark contours represent regions of steeply inclining slopes (i.e. the steep northeast slope).

TECHNIQUES

Core Collection

Jumbo piston cores were collected in the GOP aboard the RV-Melville during March and April of 2004. Sub-samples from jumbo piston cores 22 and 66 from the Moresby and Pandora trough locations of the GOP study site were collected for detrital modal analysis with the goal of relating these sediments to provenance, tectonic setting, and drainage evolution of the Southern Papua New Guinea highlands and adjacent continental shelf and slope. Core locations were selected to target specific facies, following scrutiny of Multibeam and 3.5 GHz seismic data. The ship's dynamic positioning system allowed for positive station location. Multibeam bathymetry along with seismic lines revealed JPC 66 to be located in a flat-floored basin with ponded turbidites located approximately 230 km due south-southeast of the Fly river. JPC 22 of the Moresby trough appeared to be associated with deep-sea channel levee deposits located approximately 85 km south-southwest of Port Moresby, PNG. JPC 66 is in closer proximity to the Fly, Kikori, and Purari river systems, while JPC 22 is in closer proximity to Port Moresby and the eastern Papuan Peninsula. Figure 3 displays the associated bathymetry along with the core locations and major river systems.

Shipboard Analysis

Each core was analyzed aboard the RV-Melville using a GEOTEK Multi-Sensing Core Logger (MSCL). Gamma density was measured with a narrow beam of gamma rays emitted from a 10 milli-curie ^{137}Cs source with energies principally at 661 KeV. Magnetic susceptibility was measured through a Bartington Magnetic Loop Sensor. Density and magnetic susceptibility profiles, shown in Figures 4 and 6, enable identification of sandy turbidites. Sub sampling was partially dictated by the largest observable sandy bed. With the exception of sampling intervals downcore no clear representative chronostratigraphy was initially established. JPC 66 was sub

sampled aboard ship and JPC 22 was later sampled upon arrival at the Rosentiel School of Marine and Atmospheric Science (RSMAS). Additional lab-based sampling strategies are discussed below.

Map Data

Regional geologic information and digital elevation models of the drainage basin can be utilized to make inferences about sediment sources and pathways within the hinterlands. Etopo 2 digital elevation and bathymetric data sets were used to create the counters on the location maps (Fig. 3), and the geologic interpretations are from a USGS data set (Steinshouer et al. 1999).

Lab Analysis

Sediments were sampled along the entire length of the two cores to obtain enough material to undertake petrographic (cathodoluminescence, and scanning electron microprobe), and quantitative (electron microprobe) analysis. Samples were collected from each sandy lithologic interval, each of which was the sandy basal layer of a turbidite deposit ranging from approximately 1 cm to > 100 cm. Multiple samples were acquired from each core, and analyses were concentrated on three depth intervals from varying depths within each core: a shallow interval, a mid-level interval, and a deep-level interval. The following depths were sub-sampled and analyzed: JPC 66_at 209-212, 728-744, and 857-875 cm; JPC 22_at 163-174, 300-323, and 840-844 cm. Roughly 10-20 ml of material was sampled from each interval (~ 5-15 cm along the length of the core). The sands were sieved at the very fine sand (63-125 μm) fraction, the dominant size class in most turbidites sampled. This size fraction was easily identified and sampled in the natural graded bedding (fining upwards sequence) of these modern turbidites. The sieved sediment samples were dried at 60° C and subsequently mixed with a petrographic epoxy, smeared onto a slide and allowed to cure, then thin-sectioned to a standard 30 μm thickness and polished for petrographic and electron microprobe analysis (Camuti et al. 1999).

Each sample was documented and analyzed in a number of ways. Plain light photomicrographs were taken of each sample at 5 and 10x magnification, in conjunction with cathodoluminescence (CL) images at the same magnifications. Optical CL was performed with a Technosyn cold cathode attachment on a standard petrographic microscope equipped with a camera for film imaging. The JEOL 840A scanning electron microscope at LSU was used for textural imaging of the detrital mineral grains, and backscattered electron (BSE) images in conjunction with energy dispersive spectroscopy (EDS) were used for positive grain identification. This latter feature is possible because the gray level in the BSE images are a function of the mean atomic weight of the mineral and the EDS provides a chemical fingerprint of the grain. Once grains were positively identified, Quartz-Feldspar-Lithics (QFL) ternary diagrams after Dickinson (1970, 1988) were used to define the general tectonic setting of the adjacent hinterlands**.** QFL diagrams were generated from point counts of 300 grains, with both polycrystalline and monocrystalline quartz being grouped as one component (Q), the feldspar component (F) including both plagioclase and potassium feldspar, and all other grains with the exception of biogenic carbonate tests were grouped into the lithic component (L).

This investigation also utilized the capabilities of the cathodoluminescence attachment to the JEOL 840A SEM (SEM-CL). The SEM-CL was used to reveal variability between quartz and plagioclase grains, later quantified by electron microprobe analysis. When subjected to significant excitation from an electron beam, certain minerals emit visible light due to electron excitation broadly grouped under the term “cathodoluminescence”. Cathodoluminescence scanning electron microscopy (SEM-CL) utilizes the highly stable electron beam to induce CL in the specimen. A mirror is placed above the sample in the SEM chamber reflects the light produced by CL into a dedicated detector and imaging system. The CL detector itself does not detect color. However, by placing bandpass red, green and blue gel filters between the mirror and

the detector, the separate RGB component colors could be collected and reintegrated to produce color SEM-CL images. A separate image was obtained for each component color. These images were recombined digitally using Image J and Photoshop 6.0 to produce a full color SEM-CL image.

Woody debris collected from JPC 66 and JPC 23 were sent to The National Ocean Sciences Accelerator Mass Spectrometry Facility (NOSAMS) at the Woods Hole Oceanographic Institution for analyses of ^{14}C at natural abundance levels. NOSAMS reports the results as uncorrected with an approximated error bar. For corrected age assumptions it is necessary to run the uncorrected ages through an accepted radiocarbon model, which was provided by OxCal calibration software. OxCal uses the following assumptions for determination of true age from radiocarbon: 1. the proportion of radiocarbon in the atmosphere has varied by a few percent over time, and 2. the true half-life of radiocarbon is 5730 years and not the original measured value of 5568 years. The corrected ages are reported below.

Electron Microprobe Analysis

Representative mafic silicate minerals, plagioclase feldspars and volcanic glass from cores JPC 66 and JPC 22 were quantitatively analyzed by wavelength dispersive spectrometry (WDS) withusing the JEOL 733 electron microprobe at the Department of Geology and Geophysics Microanalytical Laboratory at the LSU. WDS analyses were done at an accelerating potential of 15 kV and 6-10 nA using a 1-5 μm electron-beam diameter, with plagioclase feldspar being analyzed at 6 nA and the other minerals/glass at 10 nA. Standards were well-characterized natural minerals, including andalusite (Al), plagioclase (Al, Si), diopside (Ca, Mg, Si), fayalite (Fe), chromite (Cr), kaersutite (Ti), rhodonite (Mn), albite (Na), sanidine (K, Ba), tugtupite (Cl) and apatite (F). Secondary standards of known composition and similar

mineralogy were run simultaneously with the samples from the study, to provide a measure of the precision of the results. Amphiboles, biotites and feldspars were normalized on the basis of 23, 22 and 8 oxygens, respectively, using the STOICH software written by Darrell Henry (personal communication).

RESULTS

Bulk Density and Magnetic Susceptibility

JPC 66

Jumbo piston core 66 contains numerous sandy turbidites at uneven intervals downcore, interbedded with hemipelagic sections. The turbidites have been deposited by episodic gravity flow sedimentation through the late Quaternary to recent time. Bulk density measurements show an overall decreasing density upwards throughout the length of the core, with a maximum density of ~ 2.0 g/cc at a depth of 9 m (below sea floor). Bulk density increases downword, with fine scale variability of ~ 0.4 g/cc over distances of ~ 10-30 cm. The core consists of numerous high-density beds, interpreted as the basal portion of fine-grained sandy turbidites (Fig. 4). Magnetic susceptibility also increases with depth to a maximum of ~ 250 SI at a depth of 9 m (below sea floor). Generally, prominent peaks in the magnetic susceptibility correlate with zones of elevated density. Plates A, B, and C illustrate turbidite bed intervals that were the primary targets for extended analytical work (Figure 5).

JPC 22

Jumbo piston core 22 also contains sandy turbidites extending to the base of the core, although overall does not contain the number of large turbidite intervals as seen in JPC 66. There is an overall pattern of downward density increases with fine-scale variability of ~ 0.3 g/cc over distances of ~ 5-10 cm. Bulk density measurements also reflect overall a decreasing density upwards throughout the length of the core, with a maximum density of 1.8 g/cc at a depth of 6.5m. Magnetic susceptibility increases with depth to a maximum of ~ 50 SI at a depth of 10 m (below sea floor). Magnetic susceptibility peaks generally correlate with zones of elevated density as was observed in JPC 66 (Figure 4).

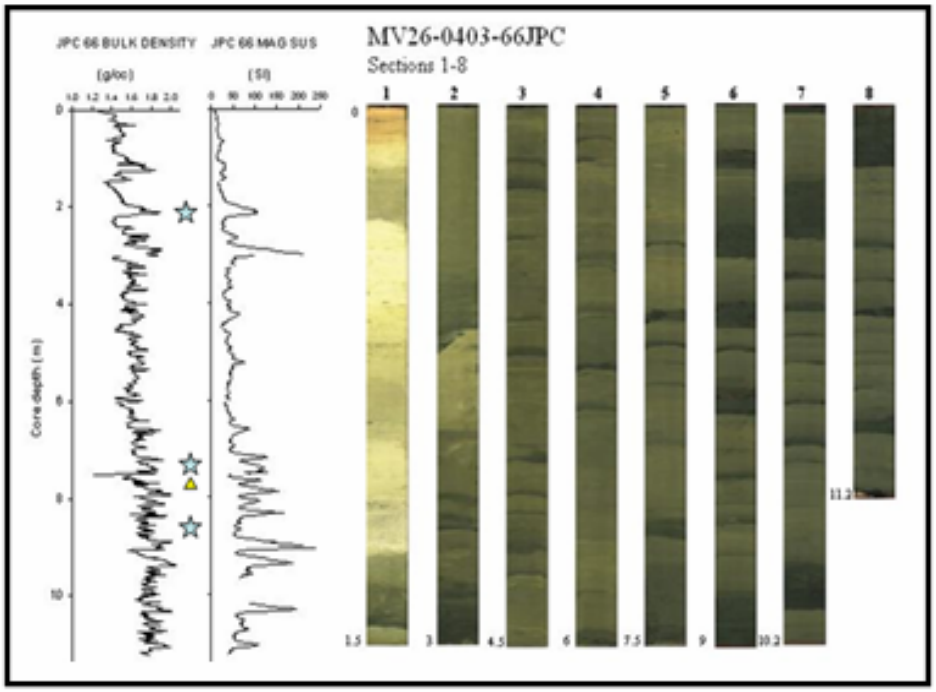

Figure 4. Bulk density, magnetic susceptibility, and Geotek core images of 66 JPC displaying multiple fine-grained sandy turbidites throughout the length of core. The logged core is from the Pandora trough with depth reported in meters. Blue stars mark depths samples for petrologic analysis. Yellow triangle marks ^{14}C sample analysis.

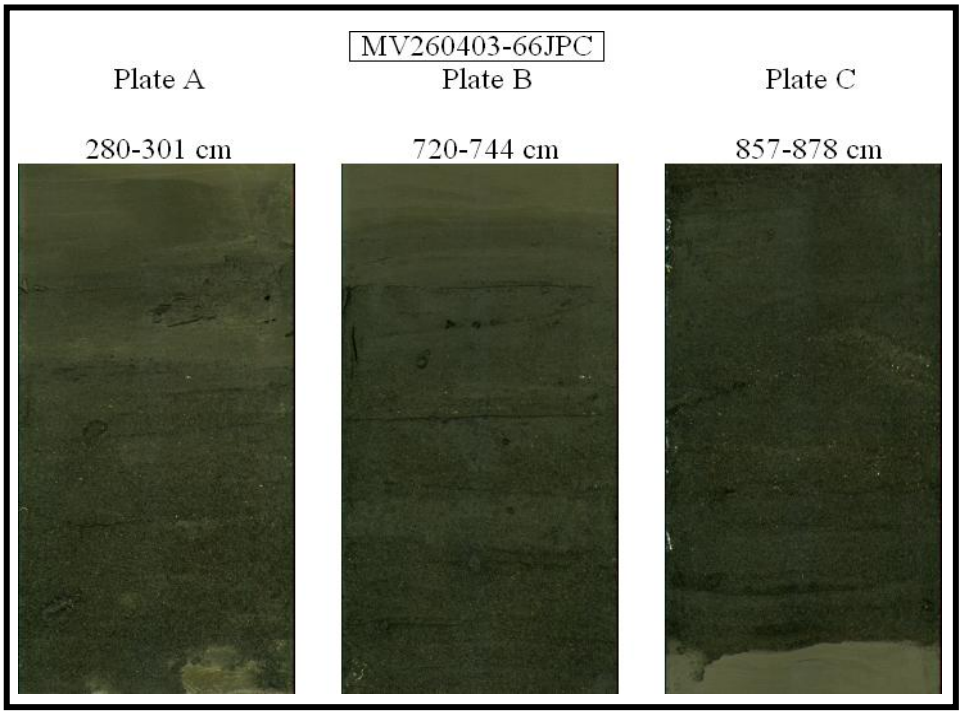

Figure 5. Plates A, B, & C showing enlarged intervals of the core displaying the fine-grained turbidites, the primary targets for analysis.

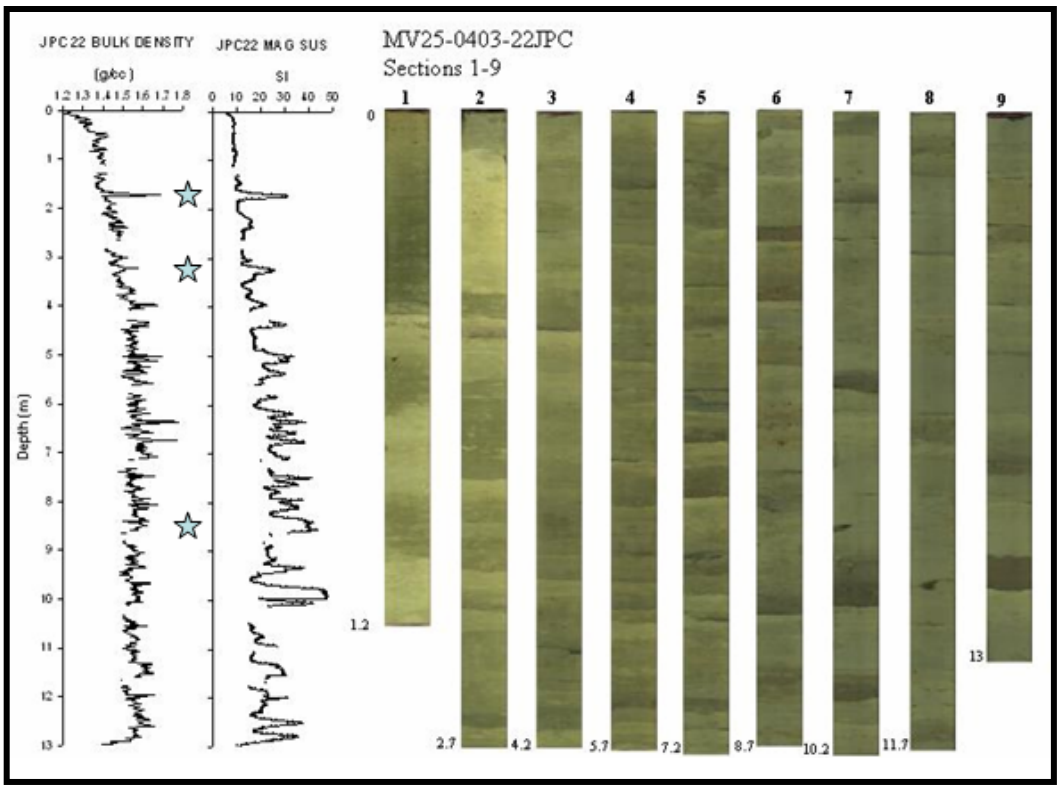

Figure 6. Bulk density, magnetic susceptibility, and Geotek core images of core 22 JPC displaying multiple fine-grained sandy turbidites throughout the length of core. The logged core is from the Moresby trough with below sea floor depth reported in meters. Blue stars mark depths samples for petrologic analysis.

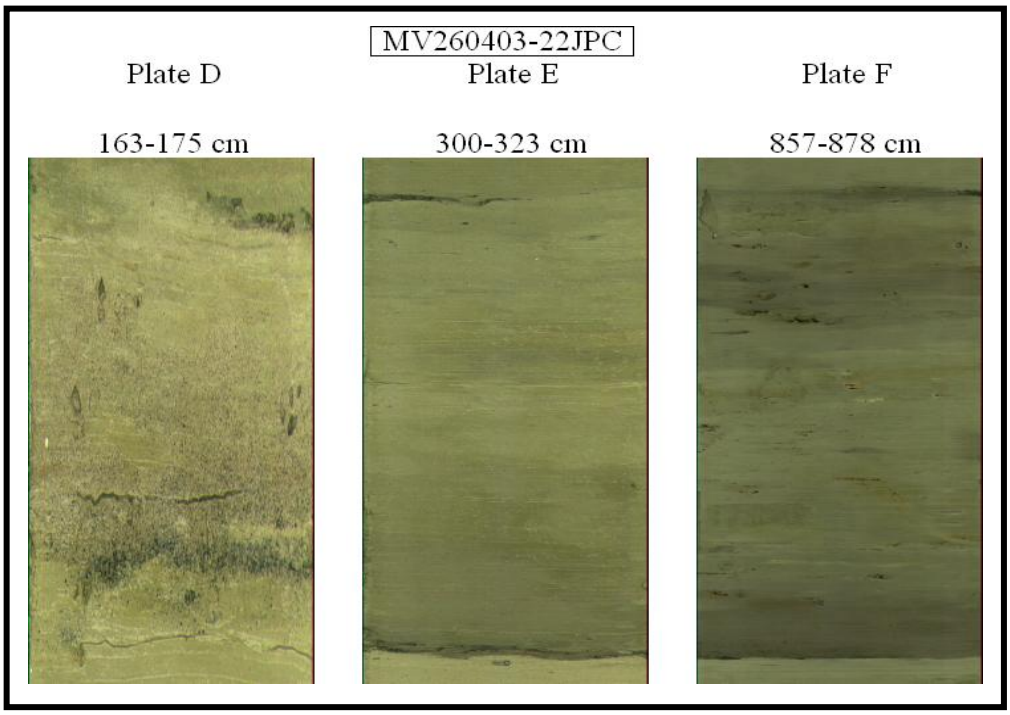

Figure 7. Plates D, E, & F showing intervals of JPC22 that contain the fine-grained turbidites with basal sands, the primary targets for analysis.

Chronostratigraphy and Sedimentation

Woody debris collected from JPC 66 and JPC 23 were analyzed for ^{14}C accelerator mass spectrometry (AMS) analysis. JPC 22 lacked any visible terrestrial organic material and only rough correlation can be made to tie this core into a chronstratigraphic framework with the other cores. A ^{14}C measurement for JPC 66 was made at a depth of 769 cm in the core and yielded a corrected age is 19,495 BP. ^{14}C analysis for JPC 23 which is located approximately halfway between 66 and 22 yielded a corrected age of 19,455 BP at a sample depth of 232 cm. Lightness data (which corresponds well to % carbonate) from a transect of cores (Fig. 8) from the GOP Study Area is plotted versus depth (personal communication from McFadden and Peterson of RSMAS).

The sedimentation rates are high in cores JPC 66 and JPC 22 in comparison to other cores in the basin. Though turbidites are common in both these cores, age dates and correlations reveal a short record in JPC 66 (769 cm of accumulation in 19,495 yrs) relative to a longer record in JPC 22 (232 cm of accumulation in 19,455 yrs), also evidenced in the increase of hemipelagic deposits in JPC 22. These observations suggest that all samples analyzed in JPC 66 are younger than Marine Isotope Stage 3 (MIS 3) (~ 45,000 to 20,000 BP), as is presumably the case in JPC 22 as well. A linear sedimentation rate for JPC 66 using the ^{14}C age measurement at a depth of 769 cm is 0.4m/1000 years for accumulation above this depth. A linear of sedimentation for JPC 23 at a depth of 232 cm is 0.12m/1000 years of accumulation above this depth. Both age measurements from JPC 66 and 23 were found to be ~ 19,500 years BP which would put this time period towards the end of the Last Glacial Maximum (LGM), but would still represent a period of sea level lowstand. The majority of accumulation above these depths would represent a period of transgressive sedimentation.

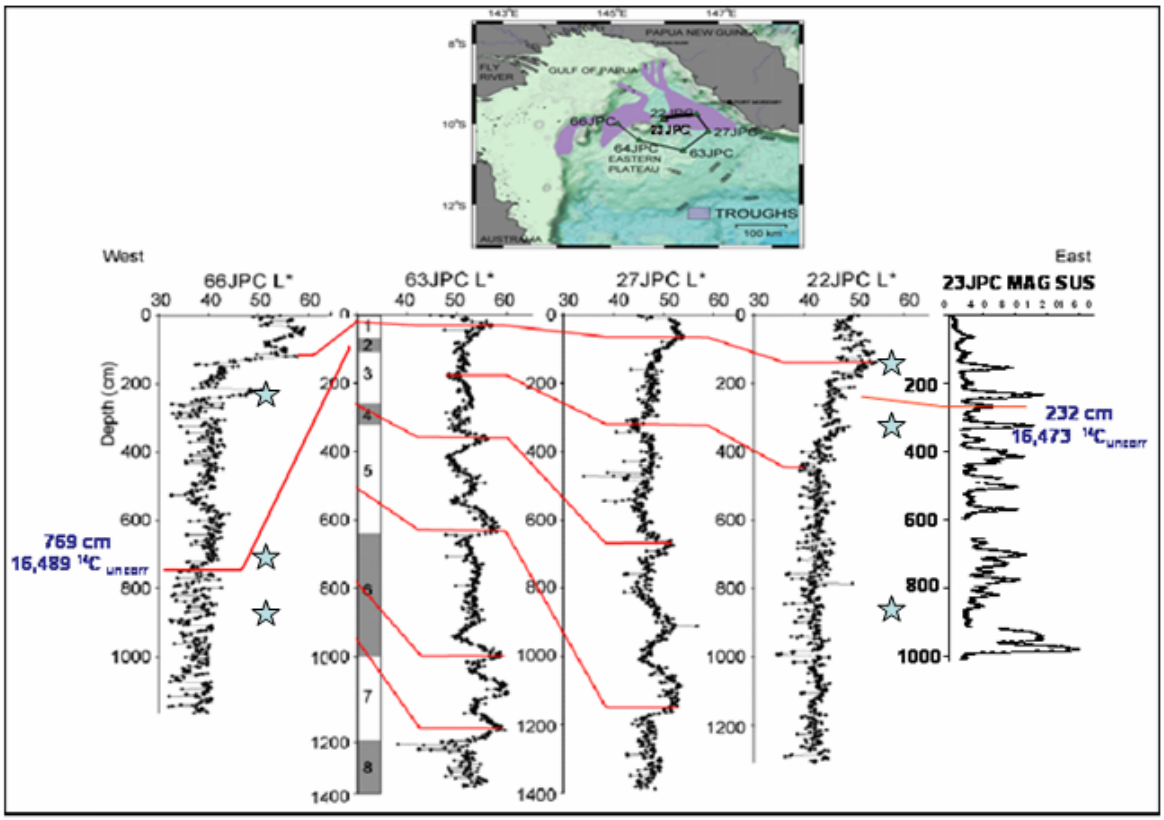

Figure 8. Chronostratigraphy and sedimentation. Lightness correlations are from Melanie McFadden and Dr. Larry Peterson of RSMAS. The vertical grey bar indicates Marine Isotope Stages, determined from oxygen isotope stratigraphy from core MV25-0403-63JPC. The uncorrected ^{14}C measurements are from cores 66 and 23 JPC. The blue stars mark thin section sample locations.

Petrographic, CL, and SEM Observations

JPC 66

The detrital mineralogy in JPC 66 is primarily quartz, with abundant K-feldspar and lesser amounts of heavy minerals (apatite & zircon) and Fe opaques minerals. Plane-polarized microscopy and optical CL for JPC 66 intervals 209-212, 728-744, and 857-875 illustrate that they are composed primarily of red-violet and red-luminescing quartz, with lesser amounts of blue luminescing plagioclase feldspars (Fig 11). Varying gray levels in the BSE images of individual grains (lighter gray grains generally being mafic grains and darker grains being quartz and feldspar) and EDS chemical data were used to identify the detritus so that accurate point

counts could be obtained. SEM analyses of JPC 66 establish that it is relatively mature quartzofeldspathic sand with the following approximate mineral modes: quartz >50%, biotite/pyroxene/amphibole ~20%, K-feldspar >10%, plagioclase < 10%, apatite < 5% and Fe-Ti Oxides (ilmenite or titanomagnetite) (e.g. Fig. 9). QFL percentages in JPC 66 are 69/14/17, 45/15/40, and 56/12/32 for intervals 209-212 cm, 728-744 cm, 857-875 cm, respectively (Fig 12). The plagioclase/total feldspar ratios are 0.47, 0.32, and 0.65 for the same respective intervals.

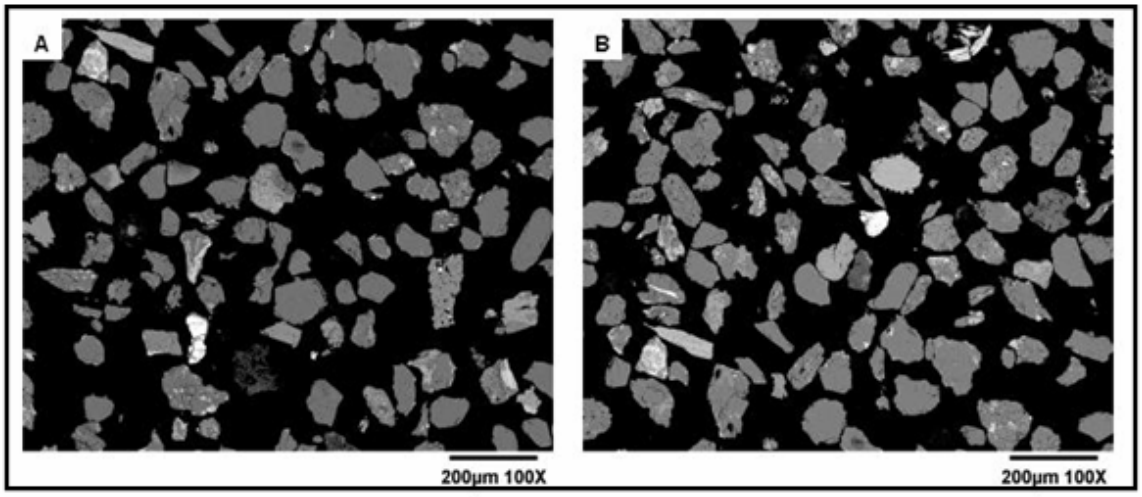

Figure 9. BSE images of sand populations in JPC 66_728-744. Variations in gray scale helped identify general grain type as well as textures. EDS chemical spectra confirmed the mineral identification.

JPC 22

Jumbo piston core 22 contains muddy and sandy turbidites throughout the core. Plane-polarized light and optical CL images generated for JPC 22 intervals 163-174, 300-323, and 840-844 illustrate the presence of a distinctly different CL grain population from that of JPC 66. This core contains green to yellow-green luminescent plagioclase feldspars with lesser amounts of blue luminescent potassium feldspars, and minimal amounts of red luminescent quartz (Fig 11). One of the most evident lithic components is brown amphibole, with lesser amounts of biotite. In

plane-polarized light the amphiboles are pleochroic from brown to light green. BSE images of the JPC 22 thin sections revealed the presence of abundant delicate skeletal, vitric pumice shards that were not obvious in plane-polarized light microscopy (Fig. 10). BSE images and EDS demonstrated that the pumice fragments were relatively Si-rich and contain phenocrysts of euhedral plagioclase, amphibole, biotite, quartz, and Fe oxides. Multiple morphologies were evident in glass fragments. Further inspection of these vitroclasts may distinguish varying glass particle morphologies as was the case seen in the Mahia Peninsula example (Schneider et al., 2001). Typical mineral modes are: sub equal parts of plagioclase feldspar/biotite/amphibole ~ 50%, pumice fragments with phenocrysts of biotite, hornblende and feldspar > 30%, quartz < 10%, apatite < 5% and Fe-Ti oxides (trace). QFL percentages are 13/64/23, 29/36/35, and 12/23/65 for intervals 163-174 cm, 300-323 cm, and 840-844 cm, respectively (Fig. 12). Plagioclase/Total Feldspar ratios are 0.90, 0.71, and 0.40 for the same respective intervals.

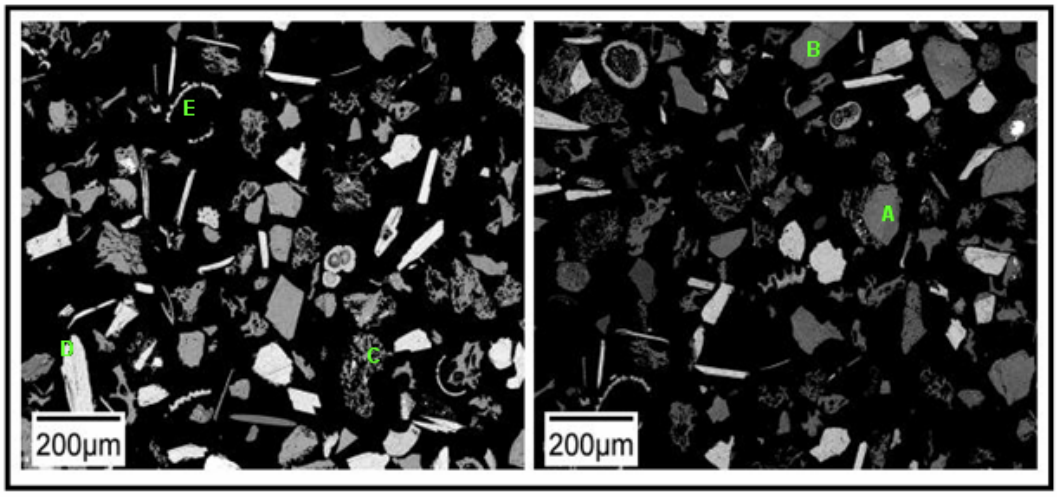

Figure 10. BSE images of sand populations in JPC 22_163-167. Variations in gray scale helped identify general grain type as well as textures. EDS chemical spectra confirmed the mineral identification. Vesicular grains represent pumice fragments and can also be seen with associated phenocrysts. Grain identification: Plagioclase as associated phenocrysts in pumice fragment (A), individual plagioclase grain (B), pumice fragment (C), amphibole (D), shell fragment (E).

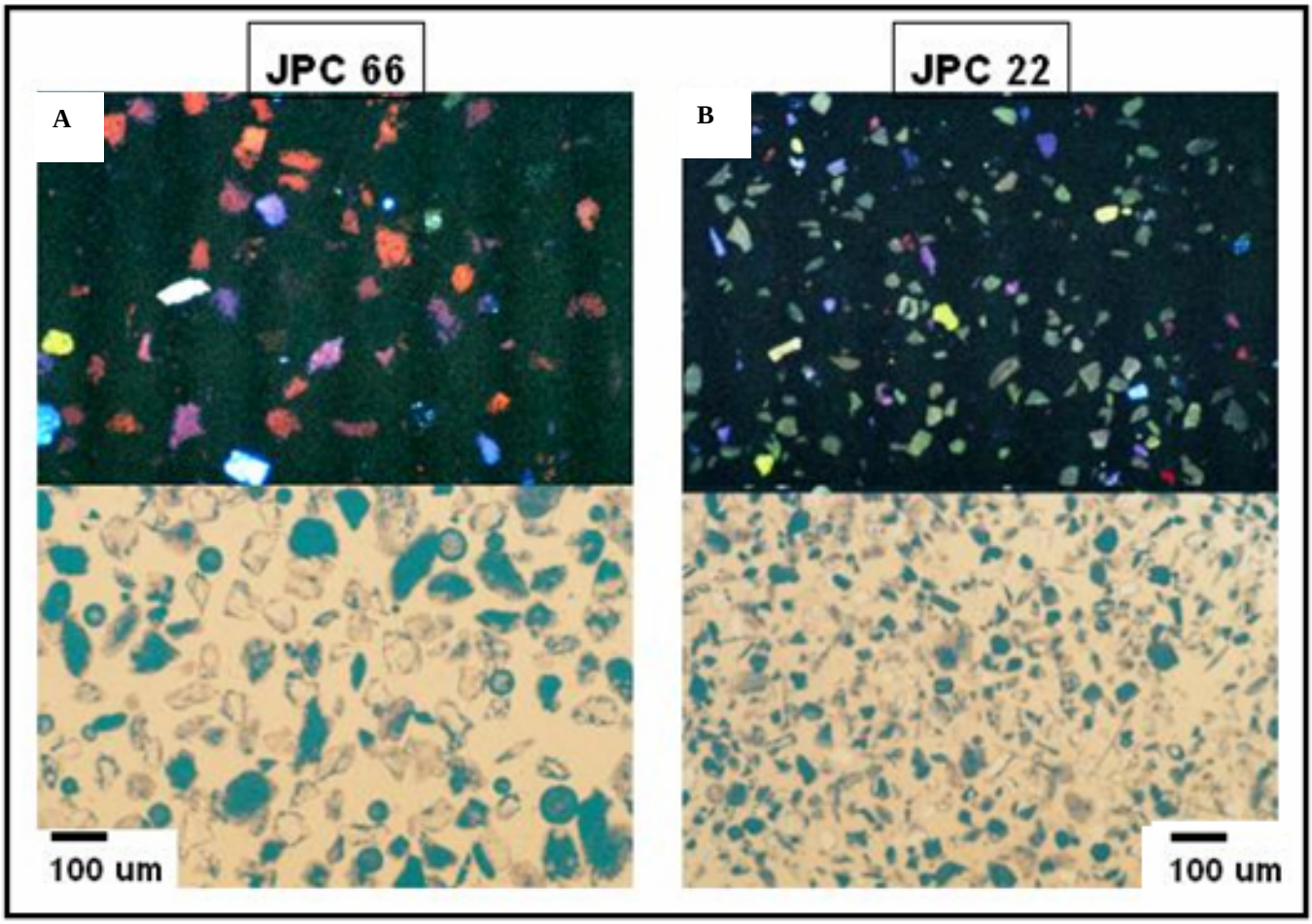

Figure 11. Plain light and optical CL images of JPC 66_209-212 (A) and JPC 22_163-174 (B). Note the distinctly different luminescence displayed between sands from the two cores.

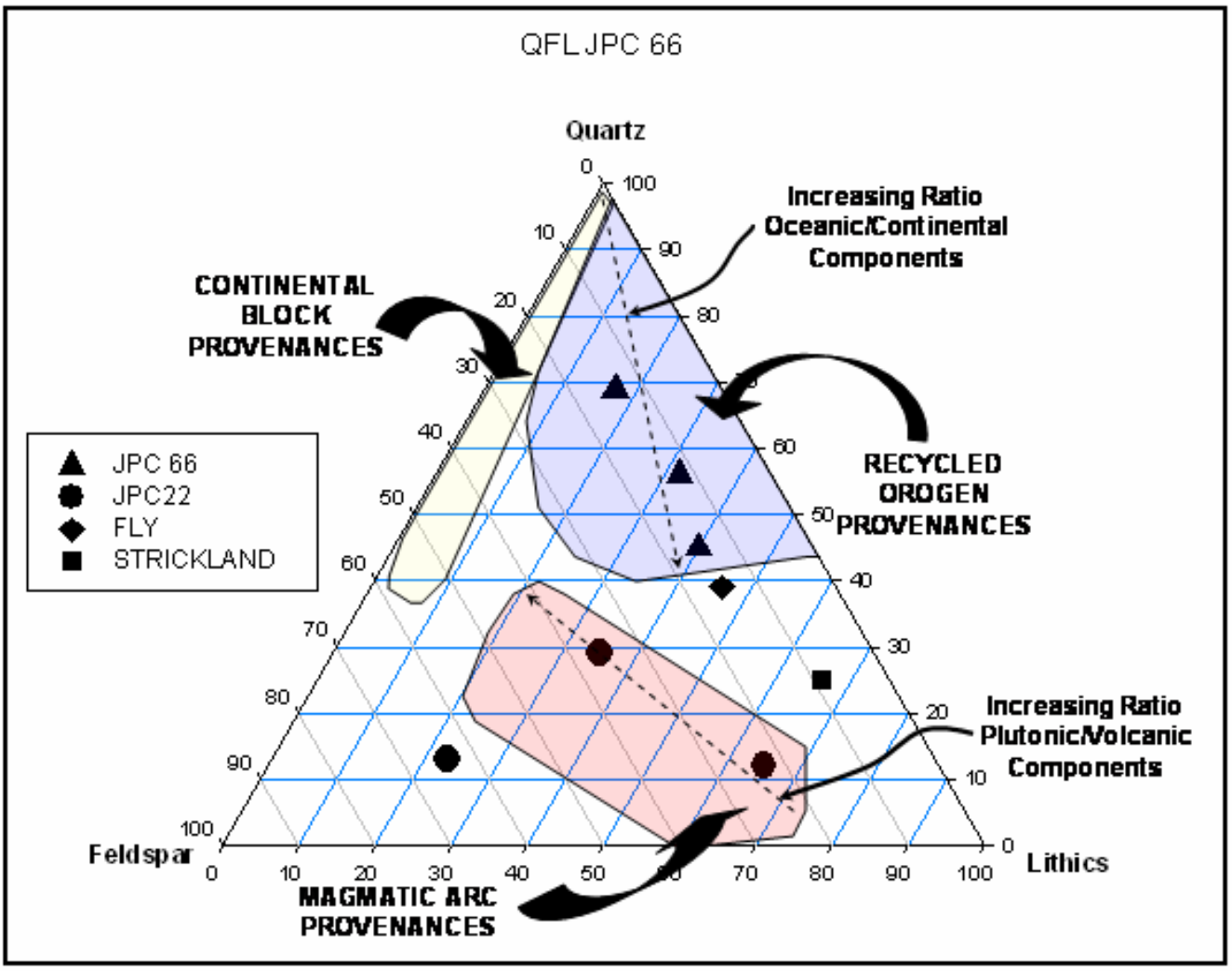

Figure 12. QFL plot of varying intervals down core in JPC22 and JPC 66. Following tectonic province nomenclature of Dickinson and Suczek, 1979 these two cores are classified as magmatic arc provenances and recycled orogen provenances, respectively.

SEM-CL Comparison Between Upper Intervals of JPC 66 & 22

SEM-CL imaging provides improved resolution of the textures and intensities of the luminescent minerals. JPC 66_300-323 and JPC 22_163-167 were examined using SEM-CL to search for textural characteristics detailing similarities between the two sand groups, primarily relating to growth or alteration history of the luminescent minerals. Plagioclase grains in samples JPC 22_163-167 and JPC 66_300-323 luminesced a strong light green under optical-Cl in contrast to the SEM-CL where the plagioclase grains were a strong red. Red luminescent

plagioclase grains with minor amounts of quartz are dominant in JPC 22; whereas blue quartz grains with lesser amount of plagioclase dominate JPC 66. Upon comparison of these two species, the plagioclase in JPC 22 is very strongly luminescent with some indication of zoning and rehealed fracturing, patterns not observed in JPC 66. Plagioclase grains observed in JPC 66 are mostly weakly luminescent. Replacement of K-Feldspar with the plagioclase is evident in the red luminescence enveloping the strong light blue luminescence.

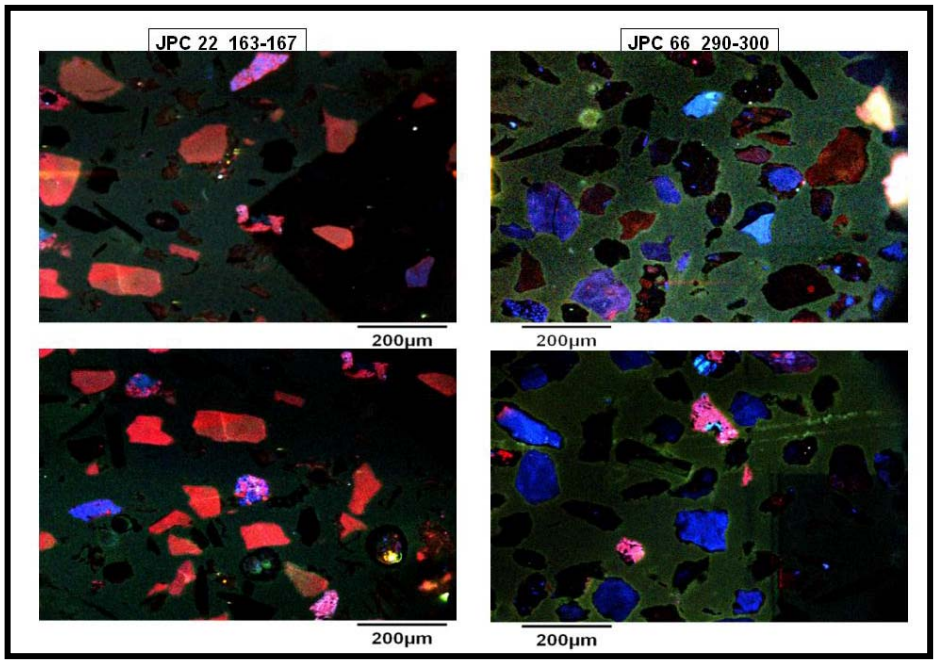

Figure 13. Scanning Electron Photomicrographs – CL of JPC 22_163-167 and JPC 66_290-300. Bright red grains are plagioclase feldspar, dark-blue grains are quartz, and lighter blue is typically K-feldspar most often associated with replacement of plagioclase.

Fly and Strickland Rivers

Plane-polarized light and optical CL petrographic observations were made for river samples from both the Fly and Strickland Rivers systems (provided by Joel Rowland of UC Berkley). One sample was analyzed from each river at each of the given locations: Fly 3 (Lat: -8º 19.2079 Long: 142º 48.0146) and Strickland (Lat: 7º 38.1770 Long: 141° 24.1850). Similar techniques for grain size, thin section preparation and QFL guidelines were followed as in each

of the piston core samples. The Fly River QFL percentages were found to be 39/15/46 while the Strickland River had percentages of 25/9/66 (Fig 12). Neither of the river samples possessed any of the pristine vitric particles that were present in the JPC 22 core, though they did possess an abundance of lithic minerals that may be volcanic in origin. The data may represent a slight bias towards the lithic end member due to mining spoils found in these river systems (primarily sulfides).

Glass and Mineral Chemistry

Volcanic glass

Electron microprobe analyses of 10 pumice glass fragments in JPC 22 163-167 establish that they are silica-rich, ranging from 75.5 to 77.7 weight % SiO_2, and have 4.9 to 7.6 weight % $Na_2O + K_2O$. A total-alkali-silica (TAS) plot of the volcanic glass within these pumice fragments is representative of a rhyolitic composition (TAS diagram, Le Bas et al., 1992) (Figure 14). Weight percent oxides values are reported in Appendix E and table 1 below.

	Volcanic Glass		Amphibole		Biotite	
Oxides	Average*	Std dev	Average	Std dev	Average	Std dev
SiO_2	76.75	0.96	42.94	1.74	36.97	0.55
Al_2O_3	13.94	1.06	10.34	2.38	13.71	0.37
Cr_2O_3	0.00	0.01	0.01	0.01	0.03	0.02
TiO_2	0.11	0.03	2.15	1.75	3.53	0.29
FeO	1.03	0.09	13.39	2.07	15.51	0.08
MnO	0.06	0.03	0.34	0.15	0.19	0.08
MgO	0.16	0.07	12.53	0.22	13.81	0.42
CaO	1.26	0.48	10.58	0.53	0.75	0.64
BaO	0.07	0.04	0.03	0.03	0.44	0.10
Na_2O	2.81	1.18	1.97	0.44	0.69	0.06
K_2O	3.81	0.68	1.00	0.71	7.95	0.64

Table 1. Average weight percent oxide values along with standard deviations for all quantitative analysis run on volcanic glass and Fe, Mg silicates found within JPC 22. (* Values normalized to 100).

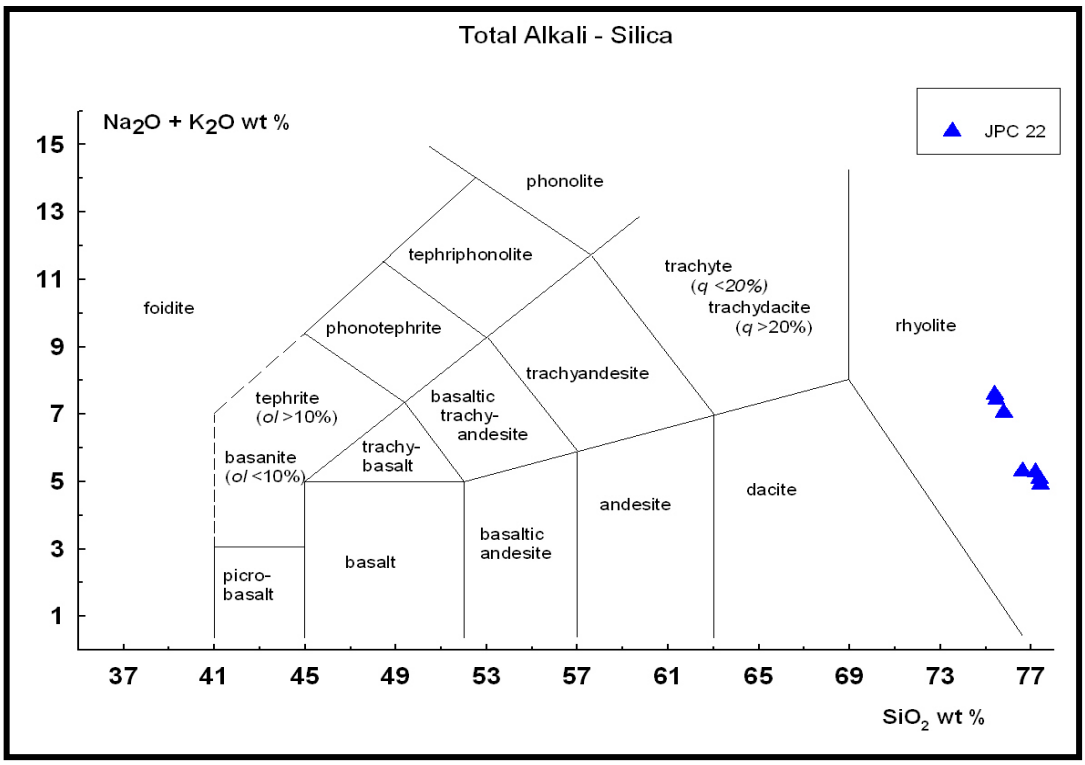

Figure 14. TAS plot of volcanic glass from pumice fragments found in JPC 22. (TAS diagram, Le Bas et al., 1992)

Amphiboles

Unaltered amphiboles are common detrital minerals in the clastic sediments of JPC 22_163-167. This core does not appear to have undergone sufficient diagenesis to alter the chemistry of the grains. Four grains from the selected intervals were analyzed and classified as edenites with Si = 6.005 – 6.749 and Mg/(Mg+Fe) = 0.595 – 0.688. At least one of the grains was contained as phenocrysts within pumice while the others were individual grains. Chemical analysis of weight percent oxides is reported in Appendix D and average values with standard deviations are reported in table 1. Hornblende compositions within JPC 22 showed little variation. The structural formula is as follows, representing a range from the low silica end-member to the high silica end-member: $(Na_{0.42}K_{0.39})(Ca_{1.56}Na_{0.34})(Mg_{2.83}Fe_{1.28}Ti_{0.53}Al_{0.44})[Si_{6.01}Al_{1.99}O_{23}](OH)_2$ to $(Na_{0.50}K_{0.12})(Ca_{1.77})(Mg_{2.88}Fe_{1.80}Ti_{0.15}Al_{0.34})[Si_{6.75}Al_{1.25}O_{23}](OH)_2$.

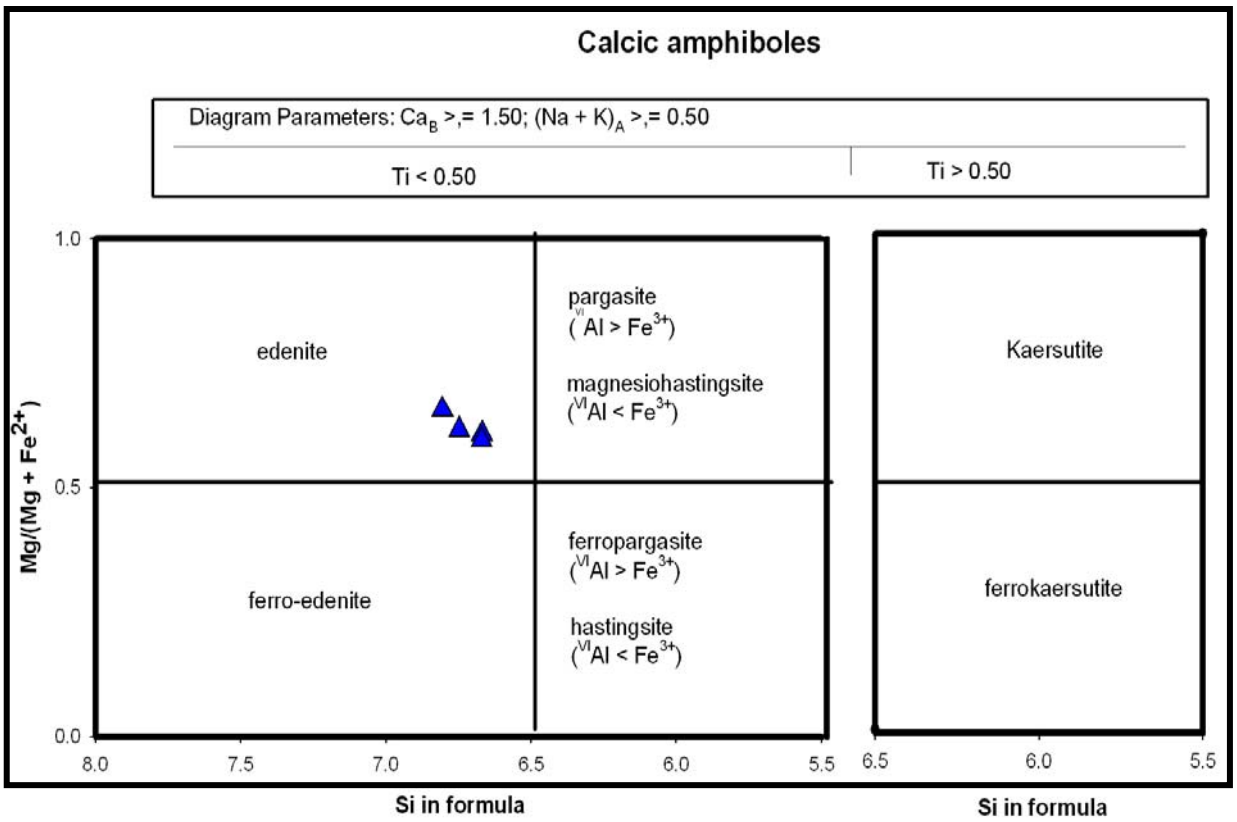

Figure 15. Classification diagram of calcic amphiboles for JPC 22 with normalization of the atomic proportions on the basis of 23 oxygens (Leake et al., 1998).

Biotites

Two biotite grains were analyzed from JPC 22, one grain from interval 163-167 and one grain from interval 300-323. Figure 16 shows the total titanium and aluminum plotted against Mg/(Mg + Fe). Biotites in JPC 22 were found as both individual grains and as associated phenocrysts within pumice fragments. Chemical analysis of weight percent oxides is reported in Appendix G and average values with standard deviations are reported in table 1. A representative structural formula for the two biotites analyzed within JPC 22 is as follows: $(K_{1.64}\ \square_{0.36})(Mg_{3.21}\ Fe^{2+}_{1.97}\ Mn^{2+}_{0.03}\ Al_{0.10}\ Ti_{0.43})\ [Si_{5.58}\ Al_{2.42}\ O_{22}]\ (OH)_4$. The biotites were found to be relatively rich in Titanium and thus could be used to calculate a minimum temperature of formation (730-740 ºC).

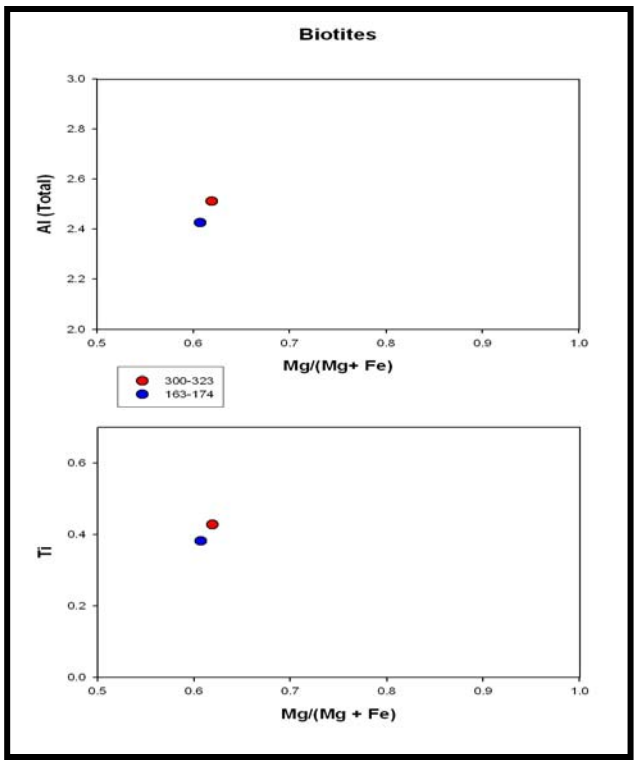

Figure 16. Biotite chemical analysis for JPC 22 intervals 163-174 and 300-323.

Plagioclase Feldspar

Plagioclase feldspar was present in all samples and can be useful to identify empirical source rock fields in the ternary system (Trevena and Nash, 1981). The distributions of plagioclase compositions in the two cores are quite distinct (Fig. 17). JPC 22 plagioclase at intervals 163-174 and 300-323 has relatively high anorthite contents that range from 33.1 to 52.6 % anorthite. In contrast, the JPC 66 plagioclase at intervals 209-212 and 728-744 have a bimodal mixture of anorthite contents with some grains being nearly pure albite 0.08 % An to calcic plagioclase with 59.6 % An. Feldspar chemistry of JPC 22 is represented as a unimodal distribution with all data points clustering at intermediate anorthite content. Two general modes can be seen for JPC 66 plagioclase feldspar chemistry. Analysis of JPC 66 intervals 300-323 and 720-729 show a bimodal distribution of with data points clustering at both intermediate anorthite content and minimum anorthite content.

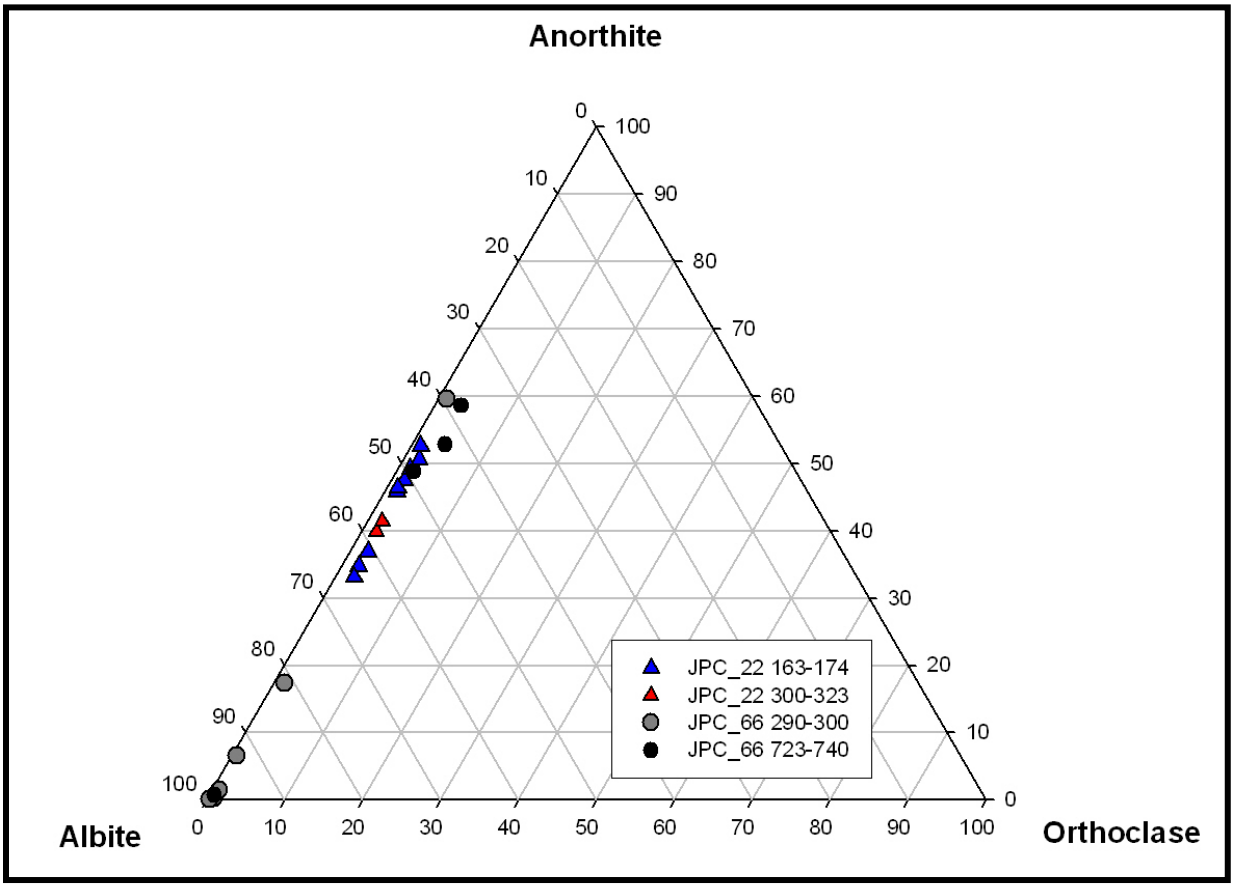

Figure 17. Ternary plot of the plagioclase feldspars, which are representative of the Albite - Anorthite ($NaAlSi_3O_8$ - $CaAl_2Si_2O_8$) solid solution plagioclase series

DISCUSSION

JPC 66 located in the Pandora trough system is in closer proximity to the Fly, Kikori, and Purari river systems than JPC 22 (Fig. 2). Radiocarbon dates along with lightness correlations indicate that a higher sediment flux from these rivers has feed the JPC 66 locality throughout much of the late Pleistocene (Fig. 8). The geomorphology of the basin does suggest that this core is somewhat isolated from the east by Eastern Fields reef and has probably not received as much sediment input from the highlands to the northeast as JPC 22 presumably has. The Moresby Trough appears to have received turbidite sands derived mostly from volcanic/collision margin highlands of SW PNG, as opposed to the Pandora Trough, which appears to be receiving more quartzose sands from the Fly/Strickland system, more akin to a trailing-edge margin. This varying mineralogy between JPC 66 and JPC 22 may also suggest multiple sources for sediments feeding JPC 66 and a single sources feeding JPC 22. Multiple sources are indicated for JPC 66 by the CL imaging, which showed variability in the presence or lack of blue luminescent potassium feldspar (most representative of a plutonic source) and varying luminescence in SiO_2 from strong red to a red-violet (suggesting mixed origin of volcanic and intrusive) (Marshall, 1988).

Volcaniclastic Turbidites

Based on the QFL plots all assemblages found in JPC 22 of the above-mentioned intervals are consistent with sediments found in back arc basins. A downcore trend of increasing ratio of volcanic/plutonic components is evident in JPC 22 (Fig. 12), similar to the observations of Dickenson and Suczek (1979). This may also suggest that volcanism influences have decreased through time. Angularity of quartz grains indicates that the source is proximal to the sample site. The chemical fingerprint of the JPC 22 sands appears to be dominated by mid to high temperature rhyolitic rock fragments, edenitic amphiboles, unimodal plagioclase feldspars,

and high Ti biotites (applying the Ti-in biotite geothermometer of Henry et al. (2005) suggests a minimum temperature of formation of these biotites to be approximately 730-740 ºC). This core appears to represent a portion of the basin in which the terrestrial input has been dominated by volcanic source delivery, most likely from small rivers throughout the late Quaternary. However, the present prevalence of hemipelagic sediments indicates that this locale is not currently being extensively fed by these source areas. The clustered nature of all the chemical data indicates that these sands are biased towards a single source component. The fairly homogeneous nature of the sands with depth also indicates that the volcanic signatures appear to be of monogenetic origin. It is unclear if the volcaniclastic material has been deposited primarily by hot subaerial pyroclastic flows directly into the GOP or if the material underwent a period of storage in the coastal plain or shelf before being remobilized and deposited on the sea-floor. What is clear is the evolution of the active volcanic arc of Papua New Guinea has influenced the adjacent deep-sea sediments of the northeastern Moresby trough, in such a way that a relatively pristine fingerprint can be seen in the volcaniclastic sands.

Turbidites Sourced from the Coastal and Deltaic Plain

Sediments in JPC 66 were also deposited from turbidity flows, although from fundamentally differing sources than JPC 22. Based on the QFL plots all assemblages found in JPC 66 were consistent with sources associated with trailing edge continental margins (Fig. 12). Increased lithic abundance down core may be evidence of inland orogenic events, or volcanism. The lack of a pristine volcaniclastic fingerprint in this region may represent a basin isolated from eastern New Guinea volcanism with more mature sediments solely derived from the south-central large coastal plain rivers. The traverse through the coastal plain rivers and across the broad continental shelf would have stripped these sands of any pristine volcanic material if it were present. Geologic information does suggest that the Fly highland province contains multiple volcanic outcrops, although the deep-sea end-member of these source rocks is not seen

in the turbidite sands sampled in JPC 66. Massive sediment flux from the GOP rivers has influenced the progradation of the southeastern PNG continental shelf (Sarg, 1988; Milliman et al., 1999). During periods of sea level low-stand, off-shelf sediment flux has been enhanced, and the signature of these riverine sediments can be recorded in the deep-sea end member as quartz-dominated turbidite deposits characteristic of this passive margin setting.

CONCLUSIONS

Piston cores from the Gulf of Papua reveal diverse sediment composition seen in the terrigenous components (fine-grained sandy turbidites) of JPC 66 and JPC 22. These sediments represent a range of siliciclastic sediments derived from multiple source regions of the hinterlands of PNG interbedded with marine-derived condensed sections representing periods of reduced turbidite deposition, thus preserving more hemipelagic rich zones. Physical log measurements revealed multiple fine-grained sandy turbidites in cores JPC 66 and JPC 22, each located south of the Gulf of Papua shelf edge. However, continental slope morphology and proximity to different upland source areas has resulted in strongly contrasting lithologies in deep-sea turbidite deposits.

Standard petrographic techniques show that deep-sea turbidites in the Pandora Trough (JPC 66), probably deposited during sea level low stands, are derived from sources most comparable to a trailing edge passive margin. In contrast, low stand turbidites (of probable low stand origin) in the Moresby Trough, represented by JPC 22, suggest provenance most comparable to a more active-back arc setting. The recognition of pristine, unaltered volcaniclastic material, primarily pumice fragments with associated phenocrysts (edenitic amphibole, plagioclase (An_{33-53}), and high Ti biotite) within JPC 22 allowed for higher resolution provenance characteristics of these sands. Vitric particles along with their associated phenocrysts revealed volcaniclastic sands of rhyolitic compositions. Plagioclase compositions in JPC 22 are consistent with a single point source for these sands. In contrast, turbidite sediments in JPC 66 lack pumice fragments, and plagioclase composition suggests a multi-genetic source. In summary, comparison of sand composition between JPC 22 and JPC 66 revealed few shared traits, suggesting that siliciclastic sources differ between the two cores. It thus follows that these multiple

fluvial sediment sources must be considered when constructing sediment budgets for the Source-to-Sink study area over timescales extending into the latest Pleistocene and earlier.

REFERENCES

Camuti, K.S. and P.T. McGuirel. (1999) Preparation of polished thin sections from poorly consolidated regolith and sediment materials. Sedimentary Geology, 128, 171-178.

Dickinson, W.R. (1970) Interpreting detrital modes of greywacke and arkose. Journal of Sedimentary Petrology, 40, 695-707.

Dickenson, W.R., Suczek C.A. (1979) Plate Tectonics and Sandstone Compositions. AAPG Bulletin. 63, 2164-2182.

Hamilton, P.J., Johnson, R.W., Mackenzie, D.E., O'Nions, R.K. (1983) Pleistocene volcanic rocks from the Fly-Highlands province of western Papua New Guinea: A note on new Sr and Nd isotopic data and their petrogenetic implications. Journal of Volcanology and Geothermal Research. 18, Issues 1-4, 449-459

Henry, D.J., Guidotti, C.V., Thomson, J.A. (2005) The Ti-saturation surface for low-to-medium pressure metapelitic biotites: Implications for geothermometry and Ti-substitution mechanisms. American Mineralogist. 90, 316 – 328.

Hovius, Niels. (2000) Macroscale process systems of mountain belt erosion. Geomorphology and Global Tectonics. 77-105.

Margasaglia, K.M., Ingersoll, R.V. (1992) Compositional trends in arc related, deep-marine sand and sandstone: A reassessment of magmatic-arc provenance. Geologic Society of America Bulletin, 104, 1637-1649.

Marshall, D.J. (1988) Cathodoluminescence of GEOLOGICAL MATERIALS. Allen & Unwin Inc. Winchester, Mass, USA.

Margins Science Plan. (2004) http://**www.margins.wustl.edu/publications/SciencePlans/**

Milliman, J.D. (1995) Sediment discharge to the ocean from small mountainous rivers: The New Guinea example. Geo-Marine Letters. 15. 127-133.

Milliman, J. D., K. L. Farnsworth, and C. S. Albertin. (1999) Flux and fate of fluvial sediments leaving large islands in the East Indies. Journal of Sea Research. 41. 97-107.

Milliman, J.D. and Syvitski, J.P.M. (1992) Geomorphic/tectonic control of sediment discharge to the ocean: the importance of small mountainous river. Journal of Geology. 100. 525-544.

Sarg, J.F. (1988) Carbonate sequence stratigraphy. In: Sea-level changes; an integrated approach. Wilgus, C.K., Hastings, B.S., Ross, C.A., Posamentier, H., Van-Wagoner, J. (eds), Special Publication - Society of Economic Paleontologists and Mineralogists. 42. 155-181.

Schneider et al (2001) Primary or secondary distal volcaniclastic turbidites: how to make the distinction? An example from the Miocene of New Zealand (Mahia Peninsula, North Island). Sedimentary Geology. 145. 1-22.

Spear, F.S., Kohn, M.J. and Cheney, J.T. (1999) P-T paths from anatectic pelites. Contributions to Mineralogy and Petrology, 134, 17-32.

Steinshouer, D.W., Qiang, J., McCabe, P.J. and R.T. Ryder. (1999) Maps showing geology, oil and gas fields, and geologic provinces of the Asia Pacific Region. U.S.G.S. Open File Report 97-470F.

Trevena, A.S., and Nash, W.P. (1981) An electron microprobe study of detrital feldspar. Journal of Sedimentary Petrology, 51, 137-150.

Valloni, Renzo., B.J. Maynard. (1981) Detrital modes of recent deep-sea sands and their relation to tectonic setting: a first approximation. Sedimentology. 28, 75-83.

Weltje, G-J, Eynatten, H-v. (2004) Quantitative provenance analysis of sediments: review and outlook. Sedimentary Geology. 171, 1-11.

Whitmore, G.P., Keith A.W. Crook, K.A.W., Johnson, D.P. (2004) Grain size control of mineralogy and geochemistry in modern river sediment, New Guinea collision, Papua New Guinea. Sedimentary Geology. 171, 129-157.

Zack T., Eynatten, H-v, Kronz, A. (2004) Rutile geochemistry and its potential use in quantitative provenance studies. Sedimentary Geology. 171, 37-58.

Zenk, M. and Schulz, B. (2004) Zoned Ca-amphiboles and related P-T evolution in metabasites from the classical Barrovian metamorphic zones in Scotland. Mineralogical Magazine, 68, 769-786.

APPENDIX A: LIST OF INTERVALS SAMPLED ABOARD RV MELVILLE 2004

Sample ID	Depth (cmbsf)	Comments
MV250403 22JPC_sec 1	0 - 46	Light hemipelagic ooze
MV250403 22JPC_sec 1	46 - 69.5	Olive clay/ooze
MV250403 22JPC_sec 1	69.5 - 90	Olive gray clay/ooze
MV250403 22JPC_sec 1	90 - 104	Light olive clay
MV250403 22JPC_sec 1	104 - 120	Light olive clay
MV250403 22JPC_sec 2	163 - 174	1st sandy turbidite with pinkish to black sandy base
MV250403 22JPC_sec_ 3	300 - 323	Black sand of basal turbidite
MV250403 22 JPC_sec_9	840 - 844	Black sand of basal turbidite

MV250403 66JPC_sec1	0 - 30	Carbonate ooze, upper 10 cm's oxidized
MV250403 66JPC_sec1	30 - 109	Light beige mud
MV250403 66JPC_sec1	109 - 123	Fine shell hash zone
MV250403 66JPC_sec1	123 - 141	Grey mud
MV250403 66JPC_sec1	141 - 144	Dark gray mud
MV250403 66JPC_sec2	144 - 150	Grey mud
MV250403 66JPC_sec2	150 - 209	Dark brown mud
MV250403 66JPC_sec2	209 - 212	Black sand
MV250403 66JPC_sec2	212 - 259	Black - dark gray mud
MV250403 66JPC_sec2	259 - 270	Interbedded black sand and mud
MV250403 66JPC_sec2	270 - 290	Mud/clay
MV250403 66JPC_sec3	290 - 301	Black sands
MV250403 66JPC_sec3	301 - 315	Mud/clay
MV250403 66JPC_sec3	315 - 324	Interbedded black sand, silt and mud
MV250403 66JPC_sec4	361 - 391	Interbedded mud and silt
MV250403 66JPC_sec4	453 -525	Mud with some silt laminations
MV250403 66JPC_sec4	525 - 527	Black sand and silt
MV250403 66JPC_sec4	527 - 600	Grey mud with some black lenses
MV250403 66JPC_sec5	600 - 604.5	Black - gray silt
MV250403 66JPC_sec5	604.5 - 662	Grey mud with black silt
MV250403 66JPC_sec5	662 - 668	Very fine grained silt
MV250403 66JPC_sec6	668 - 714.5	Dark gray silt/mud
MV250403 66JPC_sec6	706 - 708	Laminated mud and silt
MV250403 66JPC_sec7	728 - 744	Black fine sand
MV250403 66JPC_sec7	744 - 834	Interbedded gray mud with fine black silt
MV250403 66JPC_sec7	834 - 846	Fine black sand
MV250403 66JPC_sec8	846 - 857	Black clay mud
MV250403 66JPC_sec8	857 - 874	Fine black sand
MV250403 66JPC_sec9	874 - 967	Mud with small sand lenses

APPENDIX B: LIST OF INTERVALS SAMPLED POST CRUISE AT RSMAS

Sample ID	Depth (cmbsf)	Comments
MV250403 23JPC_sec2	153-155	Dark fine turbidite basal sand
MV250403 23JPC_sec3	239 - 241	Dark fine turbidite basal sand
MV250403 23JPC_sec3	329 - 331	Dark fine turbidite basal sand
MV250403 23JPC_sec4	454 - 456	Dark fine turbidite basal sand
MV250403 23JPC_sec4	484 - 486	Dark fine turbidite basal sand
MV250403 23JPC_sec4	468 - 470	Dark fine turbidite basal sand
MV250403 23JPC_sec4	521 - 523	Dark fine turbidite basal sand
MV250403 23JPC_sec7	878 - 880	Dark fine turbidite basal sand
MV250403 23JPC_sec7	926 - 928	Dark fine turbidite basal sand
MV250403 23JPC_sec7	971 - 973	Dark fine turbidite basal sand
MV250403 27TC_sec2	171-173	Dark fine turbidite basal sand
MV250403 27JPC_sec2	159 -161	Dark fine turbidite basal sand
MV250403 27JPC_sec3	247 - 249	Dark fine turbidite basal sand
MV250403 27JPC_sec3	337 - 339	Dark fine turbidite basal sand
MV250403 27JPC_sec4	431 - 433	Dark fine turbidite basal sand
MV250403 27JPC_sec4	461 - 476	Dark fine turbidite basal sand
MV250403 27JPC_sec5	546 -550	Dark fine turbidite basal sand
MV250403 27JPC_sec6	680 - 681	Pumice?
MV250403 27JPC_sec6	760 - 762	Dark fine turbidite basal sand
MV250403 27JPC_sec8	1003 - 1004	Dark fine turbidite basal sand
MV250403 27JPC_sec8	1081 - 1083	White sand lens (plank forams + quartz)
MV250403 27JPC_sec10	1289 - 1292	Dark fine turbidite basal sand

APPENDIX C: LIST OF ANALYSES PERFORMED

Sample ID	Analysis Type:					
	Petrology	QFL	CL	EDS	SEM	Microprobe
JPC 22_ 163 - 174	X	X	X	X	X	X
JPC 22_300-323	X	X	X	X	X	X
JPC 22_840 -844	X	X	X	X	X	X
JPC 23_484 - 486					X	
JPC 23_ 926 - 928					X	
JPC 27_ 159 -161	X	X		X	X	
JPC 27_ 546 - 560	X	X		X	X	
JPC 66_ 209 -212	X	X	X			
JPC 66_ 290 - 301	X	X	X	X	X	X
JPC 66_728 - 744	X	X	X	X	X	
JPC 66_834- 847	X					
JPC 66_857 - 875	X	X	X			
Fly/Strickland River	X	X	X			

APPENDIX D: AMPHIBOLE CHEMISTRY

Core	JPC 22	JPC 22	JPC 22	JPC 22
Sample Depth	163-174 cm	163-174 cm	163-174 cm	163-174 cm
Grain #	3	5	6	8
SiO_2	40.37	44.22	43.39	43.77
Al_2O_3	13.9	8.87	9.27	9.33
Cr_2O_3	0.0026	0.0065	0.0193	0.0089
TiO_2	4.77	1.2754	1.205	1.3541
FeO	10.32	14.09	14.28	14.87
MnO	0.1148	0.3963	0.3807	0.4525
MgO	12.76	12.66	12.45	12.26
CaO	9.79	10.84	10.92	10.75
BaO	0.0638	0.0428	0	0
Na2O	2.6201	1.7058	1.722	1.8188
K2O	2.0654	0.5925	0.6607	0.6657
Total	96.78	94.69	94.3	95.27
X(mm)	73.0202	63.3568	63.139	62.035
Y(mm)	11.187	69.9795	70.0487	70.1142
Date	4/4/2005	4/4/2005	4/4/2005	4/11/2005
Si	6.005	6.749	6.67	6.672
Al (vi)	1.995	1.251	1.33	1.328
Al (vi)	0.442	0.344	0.35	0.349
Cr	0	0.001	0.002	0.001
Ti	0.534	0.146	0.139	0.155
Fe^{2+}	1.284	1.798	1.836	1.896
Mn^{2+}	0.014	0.051	0.05	0.058
Mg	2.83	2.88	2.853	2.786
Ca	1.56	1.773	1.799	1.756
Ba	0.004	0.003	0	0
K	0.392	0.115	0.13	0.129
C site (M1+M2+M3)	5	5	5	5
Excess (M1+M2+M3)	0.104	0.221	0.23	0.245
Na (M4)	0.335	0.006	0	0
B site (M4) total	2	2	2.028	2.001
Na (A)	0.42	0.499	0.513	0.538
A site total	0.816	0.617	0.643	0.667
Mg/Fe (total)	2.204	1.602	1.544	1.47
Mg/Fe + Fe (total)	0.688	0.616	0.608	0.595

APPENDIX E: VOLCANIC GLASS CHEMISTRY

Core	JPC 22	JPC 22	JPC 22	JPC 22	JPC 22
Sample Depth (cm)	163-174	163-174	163-174	163-174	163-174
Grain #	1	2	3	4	5
SiO_2	71.32	72.74	71.62	77.48	76.24
Al_2O_3	13.37	13.74	13.46	12.05	11.9
Cr_2O_3	0	0	0	0	0.0027
TiO_2	0.1324	0.1316	0.1321	0.0743	0.071
FeO	0.9711	0.8721	0.9961	1.0856	1.156
MnO	0.0868	0.0702	0.0491	0	0.0554
MgO	0.1881	0.1708	0.1624	0.0383	0.0426
CaO	1.3969	1.395	1.3918	0.4081	0.431
BaO	0.099	0.0917	0.0709	0	0.0113
Na_2O	1.3182	3.62	1.4782	3.53	3.35
K_2O	3.21	3.13	3.22	4.85	5.02
Total	92.1	95.96	92.58	99.52	98.27
SiO_2	77.44	75.8	77.36	77.86	77.58
Al_2O_3	14.52	14.32	14.53	12.11	12.11
Cr_2O_3	0	0	0	0	0.0027
TiO_2	0.1437	0.1371	0.1427	0.0747	0.0723
FeO	1.0544	0.9088	1.0759	1.0909	1.1764
MnO	0.0942	0.0731	0.053	0	0.0564
MgO	0.2042	0.178	0.1754	0.0384	0.0434
CaO	1.5167	1.4536	1.5033	0.4101	0.4385
BaO	0.1075	0.0955	0.0766	0	0.0115
Na_2O	1.4313	3.77	1.5966	3.55	3.4
K_2O	3.48	3.26	3.48	4.87	5.11
Total	100	100	100	100	100
X (mm)	63.2825	63.383	63.3385	71.941	72.2232
Y (mm)	70.0392	70.076	70.071	6.83	7.1842
Date	4/4/2005	4/4/2005	4/4/2005	4/4/2005	4/11/2005

Core	JPC 22	JPC 22	JPC 22	JPC 22
Sample Depth (cm)	163-174	163-174	163-174	163-174
Grain #	6	7	8	9
SiO_2	69.72	71.01	64.66	72.91
Al_2O_3	13.55	13.4	12.15	13.8
Cr_2O_3	0.0187	0	0	0
TiO_2	0.0961	0.1313	0.0883	0.104
FeO	0.9672	0.8711	0.8358	0.9205
MnO	0.075	0.0446	0.0641	0.0413
MgO	0.1924	0.2065	0.1758	0.1904
CaO	1.44	1.3939	1.2877	1.3545
BaO	0.1188	0.0549	0.0819	0.0593
Na_2O	1.6087	3.73	1.3303	4.07
K_2O	3.21	3.26	3.09	3.26
Total	91	94.1	83.77	96.71
SiO_2	76.62	75.46	77.19	75.4
Al_2O_3	14.89	14.24	14.5	14.27
Cr_2O_3	0.0206	0	0	0
TiO_2	0.1056	0.1396	0.1054	0.1076
FeO	1.0628	0.9258	0.9977	0.9518
MnO	0.0825	0.0474	0.0766	0.0427
MgO	0.2114	0.2195	0.2099	0.1969
CaO	1.5823	1.4814	1.5372	1.4006
BaO	0.1305	0.0583	0.0978	0.0613
Na_2O	1.7677	3.96	1.588	4.21
K_2O	3.53	3.47	3.69	3.37
Total	100	100	100	100
X (mm)	62.387	62.3158	62.7238	62.78
Y (mm)	70.2605	70.309	70.705	70.6675
Date	4/11/2005	4/11/2005	4/11/2005	4/11/2005

APPENDIX F: PLAGIOCLASE FELDSPAR CHEMISTRY

Core	JPC 22	JPC 22	JPC 22	JPC 22	JPC 22	JPC 22
Sample Depth (cm)	163-167	163-167	163-167	163-167	163-167	163-167
Grain #	1	2	3	4	5	7
SiO_2	55.65	55.58	55.18	59.44	59.66	56.29
Al_2O_3	26.94	27.61	27.55	24.98	25.28	27.32
CaO	9.22	9.75	9.89	7.04	6.84	9.58
BaO	0.0806	0.0441	0	0.0508	0.0363	0.0008
Na_2O	5.87	5.78	5.48	7.08	7.36	5.97
K_2O	0.249	0.2731	0.237	0.3533	0.4145	0.2354
Total	98.01	99.03	98.34	98.94	99.58	99.39
X (mm)	61.9367	62.2829	62.7197	63.2127	63.1042	62.8857
Y (mm)	70.466	70.6345	69.6948	70.0335	70.2385	70.2315
Date	5/11/2005	5/11/2005	5/11/2005	5/11/2005	5/11/2005	5/11/2005
	Atomic proportions on the basis of 8 oxygens--					
Si	2.549	2.523	2.521	2.676	2.67	2.543
Al	1.454	1.477	1.483	1.325	1.33	1.455
Ca	0.452	0.474	0.484	0.34	0.328	0.464
Ba	0.001	0.001	0	0.001	0.001	0
Na	0.521	0.509	0.485	0.618	0.639	0.523
K	0.015	0.016	0.014	0.02	0.024	0.014
Anorthite	45.71	47.44	49.23	34.69	33.1	46.36
Albite	52.67	50.9	49.36	63.14	64.45	52.28
Orthoclase	1.47	1.58	1.4	2.07	2.39	1.36

Core	JPC 22	JPC 22	JPC 22	JPC 22	JPC 66
Sample Depth (cm)	163-167	163-167	300-323	300-323	290-301
Grain #	8	9	10	13	14
SiO_2	53.99	53.99	57.36	56.67	67.7
Al_2O_3	27.84	28.2	25.91	25.77	19.02
CaO	10.43	10.7	8.07	8.1	0.0606
BaO	0.0151	0.0167	0.02	0.0303	0
Na_2O	5.4	5.2	6.53	6.15	10.63
K_2O	0.2056	0.1943	0.3174	0.3083	0.1242
Total	97.89	98.3	98.2	97.03	97.53
X (mm)	61.9739	62.4624	16.8374	17.1944	15.7997
Y (mm)	70.7833	71.2528	39.798	39.824	70.1043
Date	5/11/2005	5/11/2005	5/11/2005	5/11/2005	5/11/2005
	Atomic proportions on the basis of 8 oxygens--				
Si	2.486	2.476	2.612	2.609	3.018
Al	1.511	1.524	1.39	1.398	0.999
Ca	0.515	0.526	0.394	0.4	0.003
Ba	0	0	0	0.001	0
Na	0.482	0.462	0.576	0.549	0.919
K	0.012	0.011	0.018	0.018	0.007
Anorthite	51	52.59	39.81	41.31	0.31
Albite	47.78	46.25	58.29	56.76	98.93
Orthoclase	1.2	1.14	1.86	1.87	0.76

Core	JPC 66	JPC 66	JPC 66	JPC 66	JPC 66
Sample Depth (cm)	300-323	300-323	300-323	300-323	300-323
Grain #	1	2	3	4	5
SiO_2	68.14	67.79	52.54	63.6	66.33
Al_2O_3	19.72	20.41	29.86	22.79	21.08
CaO	0.01	0.33	12.77	3.74	1.43
BaO	0.03	0.01	0	0	0
Na_2O	12.04	11.31	4.66	9.65	11.06
K_2O	0.07	0.16	0.18	0.23	0.1
Total	100	100	100.01	100.01	100
Date	1/11/2006	1/11/2006	1/11/2006	1/11/2006	1/11/2006
	Atomic proportions on the basis of 8 oxygens--				
Si	2.981	2.962	2.386	2.811	2.912
Al	1.017	1.051	1.598	1.187	1.091
Ca	0	0.015	0.621	0.177	0.067
Ba	0	0	0	0	0
Na	1.021	0.958	0.41	0.827	0.941
K	0.004	0.009	0.01	0.013	0.006
Anorthite	0.03	1.56	59.64	17.42	6.63
Albite	99.57	97.54	39.38	81.32	92.81
Orthoclase	0.36	0.36	0.98	1.27	0.056

Core	JPC 66	JPC 66	JPC 66	JPC 66
Sample Depth (cm)	728-744	728-744	728-744	728-744
Grain #	6	7	8	9
SiO_2	55.5	67.92	52.49	54.51
Al_2O_3	27.93	19.81	29.74	28.62
CaO	10.4	0.16	12.61	11.11
BaO	0.01	0.05	0.04	0.03
Na_2O	5.77	11.95	4.52	5
K_2O	0.39	0.11	0.6	0.73
Total	100	100	100	100
Date	1/11/2006	1/11/2006	1/11/2006	1/11/2006
	Atomic proportions on the basis of 8 oxygens--			
Si	2.503	2.974	2.388	2.466
Al	1.485	1.022	1.595	1.526
Ca	0.503	0.008	0.615	0.538
Ba	0	0.001	0.001	0.001
Na	0.505	1.014	0.399	0.439
K	0.022	0.006	0.035	0.042
Anorthite	48.82	0.74	58.6	52.81
Albite	49.01	98.59	38.01	43.01
Orthoclase	2.15	0.59	3.32	4.13

APPENDIX G: BIOTITE CHEMISTRY

Core	JPC 22	JPC 22
Sample Depth (cm)	163-174	300-323
Grain #	11	8
SiO_2	37.36	36.58
Al_2O_3	13.45	13.97
Cr_2O_3	0.04	0.0128
TiO_2	3.32	3.73
FeO	15.57	15.45
MnO	0.13	0.2457
MgO	13.51	14.11
CaO	1.2	0.2946
BaO	0.37	0.516
Na_2O	0.73	0.6431
K_2O	7.5	8.4
Total	95.57	93.96
X (mm)	62.5328	63.029
Y (mm)	70.4502	73.4417
Date	4/11/2005	3/28/2005
	Atomic proportions on the basis of 22 oxygen's--	
Si	5.718	5.583
Al (iv)	2.282	2.417
Al (vi)	0.144	0.096
Cr	0.005	0.002
Ti	0.382	0.428
Fe^{2+}	1.993	1.972
Mn^{2+}	0.017	0.032
Mg	3.083	3.21
Ca	0.197	0.048
Ba	0.022	0.031
Na	0.216	0.19
K	1.464	1.636
Oct Total	5.625	5.74
Alk Total	1.899	1.905
Mg/Mg+Fe (total)	0.607	0.619

VITA

Luke Jeremiah Patterson was born May 18, 1979, in Pasadena, California. He was raised in Ventura, California, and graduated from Buena High School in June 1997. He was then enrolled as a student at Ventura Community College where he also played football. He received a football scholarship to attend Lambuth University in Jackson, Tennessee, where he played through is fourth year, majoring in chemistry. Luke was married to his wife Harmony in the fall of 2001 and transferred to Louisiana State University in the spring of 2002, where he received a Bachelor of Science degree in geology in the fall of 2003. Luke entered the master's degree program in the Department of Oceanography and Coastal Sciences in the spring of 2004 to study under Dr. Sam Bentley. During the summer of 2005, Luke participated in an internship with Shell Exploration and Production Company in New Orleans, Louisiana. Luke is the father of three healthy and beautiful children.

.